

## Chapter 4

### Results and Discussion

Twelve compounds were isolated from the stem bark of *Glyptopetalum sclerocarpum* Laws. and three semi-synthetic compounds were obtained by acid-rearrangement reaction. Their chemical structures were discussed and except compounds GS-Y2-5, GS-Y2-6 and GS-Y3-2 were reported for their lipophilicity and biological activities (BSL and antimicrobial activity). The relationships among their bioactivities, chemical structures and lipophilicity would be suggested.

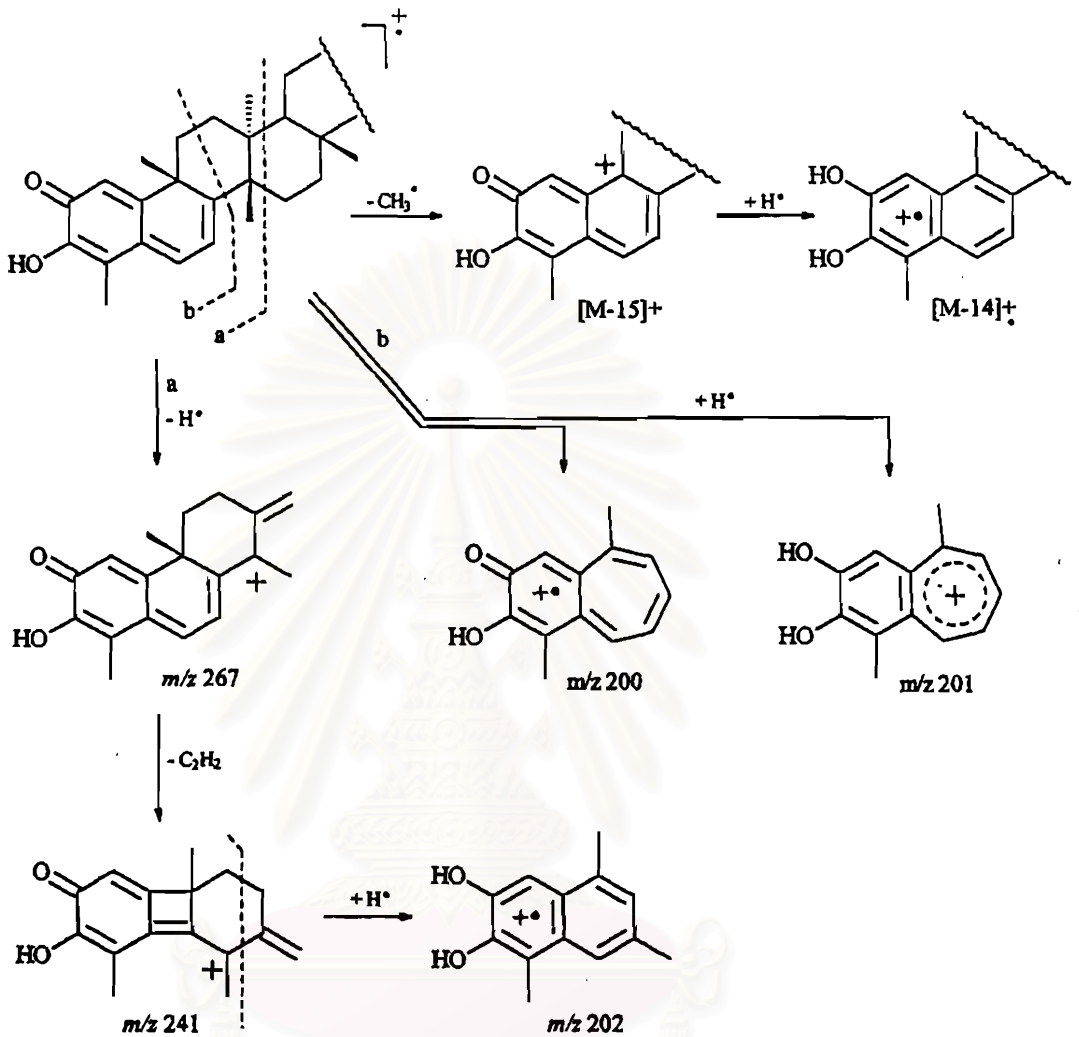
#### 1. Structure elucidation of the isolated and acid-rearranged compounds

To elucidate the structures of the isolated and acid-rearranged compounds, UV, IR, MS and extensive NMR experiments were examined. Careful analysis of splitting patterns of  $^1\text{H}$  NMR signals, their *NOEs* and Chem3D computer program (using MM2 force field) were utilized to define the most stable molecular conformation and complete NMR assignment of each compound.

##### 1.1) Structure elucidation of isolated compounds

All isolated compounds displayed similar UV absorption spectra, mass fragmentation patterns, and  $^1\text{H}$  and  $^{13}\text{C}$  NMR signals in the downfield region, all of which signified the basic structure of quinone-methide triterpenes. The mass fragmentation pattern was summarized in Scheme 18<sup>116</sup>. Extensive NMR experiments, particularly the  $^1\text{H}$ - $^{13}\text{C}$  long-range correlations examined by HMBC technique, also supported this conclusion. Some of those correlations found in all compounds were shown in Figure 3. The main structural configuration of all compounds, by NOESY experiment, was clearly shown in Figure 4. Consequently, the conformation of ring C and D were forced to be chair/chair by the rigidity of ring A and B.

The difference among these compounds was only in ring E. Their structure elucidation would be discussed consecutively.



Scheme 18. Characteristic mass fragmentation pattern of quinone-methide triterpenes.

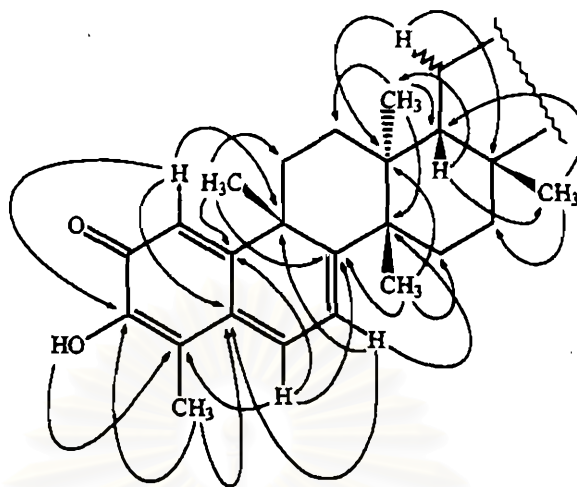


Figure 3. <sup>1</sup>H-<sup>13</sup>C HMBC long-range correlations observed in a part of the main structure of all isolated compounds.

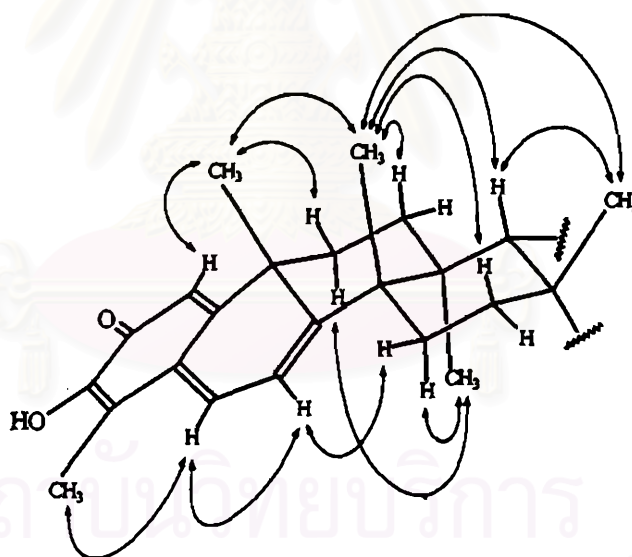


Figure 4. Some important NOE observations in a part of the main structure of all isolated compounds.

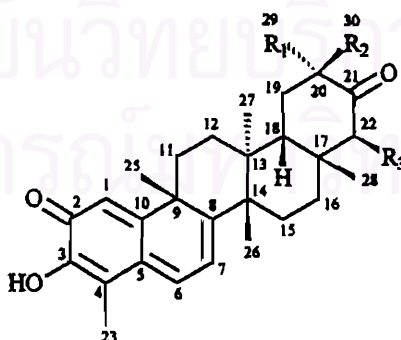
### 1.1.1) Identification of GS-T-1 and GS-Y1-1

Compounds GS-T-1 and GS-Y1-1 displayed identical melting points, *R<sub>f</sub>* values, and <sup>1</sup>H (Figure 43, page 155, and Figure 62, page 177) and <sup>13</sup>C NMR data (Figure 44, page 157, and Figure 63, page 179) to the two compounds previously found from this plant, 22β-hydroxy-tingenone (1)<sup>13</sup> and 20-hydroxy-20-epi-tingenone (2)<sup>14</sup>, respectively. Thus, discussion on their structures would be neglected. Their <sup>1</sup>H and <sup>13</sup>C NMR assignments were shown in Tables 4 and 5 (page 82-83).

### 1.1.2) Identification of GS-T-2

The molecular formula of GS-T-2 was determined to be C<sub>28</sub>H<sub>36</sub>O<sub>3</sub> from the evidence of its <sup>13</sup>C NMR (Figure 49, page 162) and MS (Figure 47, page 159) data. GS-T-2 was similar to GS-T-1 in its <sup>1</sup>H NMR spectrum (Figure 48, page 160), except that there were two methylene proton signals at δ1.86 and 2.92 ppm, instead of a methine proton signal, on C-22 position. The C-22 signal (δ 52.5 ppm) was more upfield than that of GS-T-1 (δ 76.4 ppm), but very close to that of GS-Y1-1 (δ 50.4 ppm), indicating that GS-T-2 should be the parent compound of GS-T-1 and GS-Y1-1, named tingenone (15).

The melting point, <sup>1</sup>H and <sup>13</sup>C NMR data of GS-T-2 were identical with those previously published of tingenone (15)<sup>116,155</sup>. Thus, it was undoubtedly identified as this known compound. Its <sup>1</sup>H and <sup>13</sup>C NMR assignments were shown in Tables 4 and 5 (page 82-83).



	R <sub>1</sub>	R <sub>2</sub>	R <sub>3</sub>
(1) GS-T-1	H	CH <sub>3</sub>	OH
(15) GS-T-2	H	CH <sub>3</sub>	H
(2) GS-Y1-1	CH <sub>3</sub>	OH	H

### 1.1.3) Structure elucidation of GS-Y1-2

GS-Y1-2 exhibited MS (Figure 66, page 181) and  $^{13}\text{C}$  NMR (Figure 68, page 184) data corresponding to the molecular formula  $\text{C}_{28}\text{H}_{36}\text{O}_4$ . Its  $^{13}\text{C}$  NMR spectrum was very similar to that of GS-Y1-1 (Figure 63, page 179). A methylene carbon ( $\delta$  47.8 ppm) was proved to be on C-22 position, according to the HMBC experiment (Figure 71, page 187-189, or summarized in Figure 5). It showed three-bond correlations to H-16 $\beta$  ( $\delta$  1.88 ppm), H-18 ( $\delta$  1.75 ppm) and 3H-28 ( $\delta$  1.28 ppm). The fact that all methyl signals in its  $^1\text{H}$  NMR spectrum (Figure 67, page 182) were singlet and result from DEPT experiment (Figure 68, page 184) supported the assignment of C-20 as a quaternary carbon. Based on its downfield shift in the  $^{13}\text{C}$  NMR spectrum ( $\delta$  72.0 ppm), a hydroxyl group should be placed at this position. The three-bond correlation of C-19 ( $\delta$  34.5 ppm) to this hydroxyl proton ( $\delta$  3.06 ppm) also confirmed this suggestion. The hydroxyl and methyl protons also displayed three-bond correlations to a carbonyl carbon at  $\delta$  216.3 ppm, which, alternately, showed two-bond correlation to H-22 $\alpha$  ( $\delta$  2.75 ppm) and H-22 $\beta$  ( $\delta$  2.17 ppm).

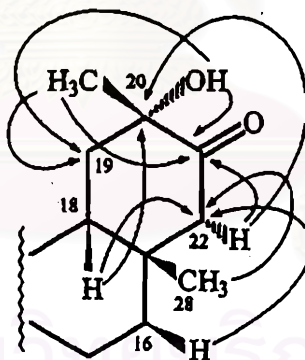


Figure 5. Some important  $^1\text{H}$ - $^{13}\text{C}$  HMBC long-range correlations in ring E of GS-Y1-2.

Therefore, the gross structure of GS-Y1-2 should be the 20-OH, 21-oxo quinone-methide triterpene, surprisingly identical to that of GS-Y1-1. However, the NOEs observed between 20- $\text{CH}_3$  and 17- $\text{CH}_3$ , and between 20-OH and 13- $\text{CH}_3$  (Figure 6, and Figure 72, page 190) clearly indicated GS-Y1-2 to be 20-epimeric stereoisomer of GS-Y1-1, named 20-hydroxy-tingenone (45). Its  $^1\text{H}$  and  $^{13}\text{C}$  NMR assignments were shown in Tables 4 and 5 (page 82-83).

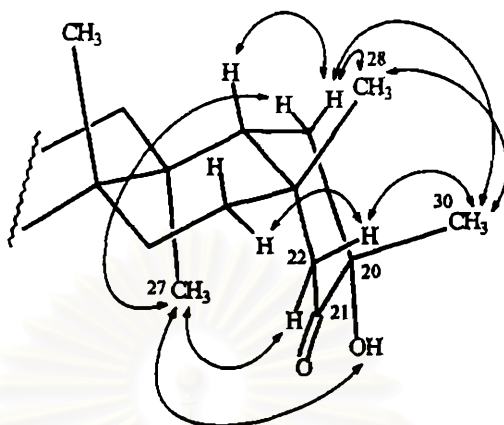
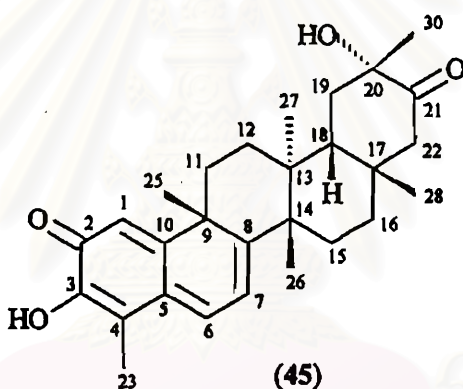
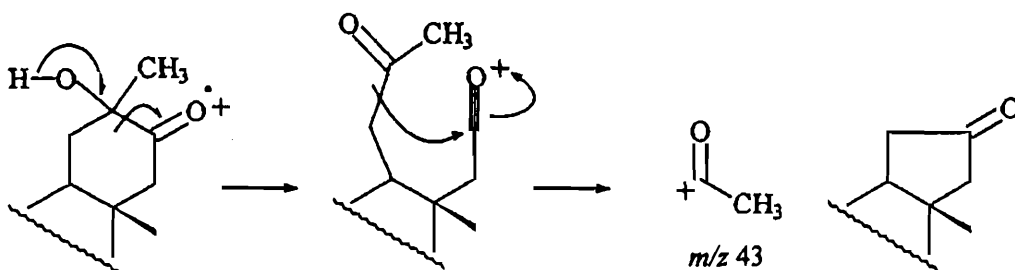


Figure 6. Conformation and selected NOEs in ring E of GS-Y1-2.



There was a relatively high intensity peak at  $m/z$  43 in both mass spectra of GS-Y1-1 (Figure 61, page 176) and GS-Y1-2 (Figure 66, page 181). Fragmentation pattern of this significant fragment was suggested in Scheme 19. It confirmed the proposed substructure of a carbonyl group adjacent to a quaternary carbon which was geminally substituted with a methyl and a hydroxyl group.



Scheme 19. Proposed mass fragmentation pattern of mass fragment at  $m/z$  43.

A significant difference between  $^1\text{H}$  NMR spectra of GS-Y1-1 (Figure 62, page 177) and GS-Y1-2 (Figure 67, page 182) was the chemical shift of their 3H-27 which were at  $\delta$  0.89 and 0.62 ppm, respectively. This could be explained by their ring E conformation. In GS-Y1-2, the *NOE* observed between 3H-30 and H-22 $\beta$  but not between 20-OH and H-22 $\alpha$ , indicated ring E to be in boat conformation (Figure 6). It was also confirmed by the result calculated by MM2 force field (Figure 7). In this conformation, the anisotropic effect of the 21-carbonyl group would easily influence on the 3H-27 and cause the signal to be more upfield.

The structure of GS-Y1-1 (2) had been assumed to be GS-Y1-2, but later, Likhitwitayawuid et al revised it as the correct structure <sup>2</sup>. Therefore, this was the first time that 20-hydroxy-tingenone has been found to occur naturally.

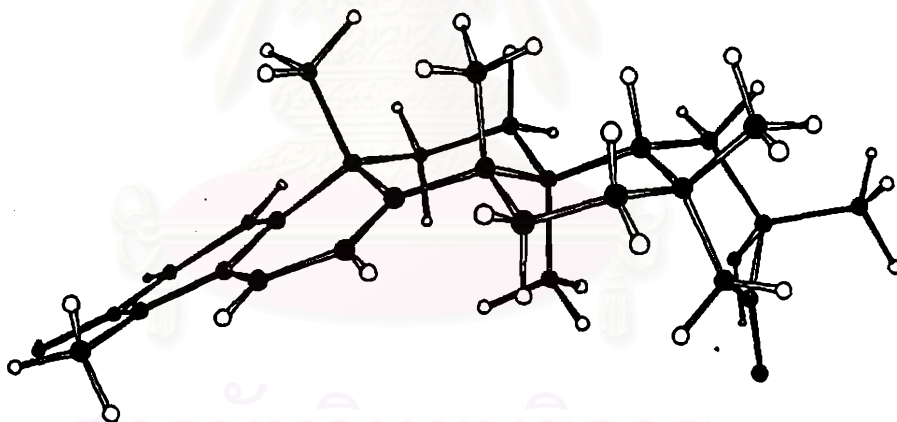


Figure 7. Most stable conformation of GS-Y1-2, calculated by MM2 force field (52.237 kcal/mole).

Table 4. <sup>1</sup>H NMR assignments of GS-T-1 (1), GS-T-2 (15), GS-Y1-1 (2) and GS-Y1-2 (45).\*

Proton	GS-T-1 (1)	GS-T-2 (15)	GS-Y1-1 (2)	GS-Y1-2 (45)
1	6.54 ( <i>d</i> ; 1.5)	6.55 ( <i>d</i> ; 1.5)	6.54 ( <i>d</i> ; 1.4)	6.51 ( <i>d</i> ; 1.5)
6	7.05 ( <i>dd</i> ; 7.1, 1.5)	7.04 ( <i>dd</i> ; 7.0, 1.5)	7.02 ( <i>dd</i> ; 1.4, 7.0)	7.01 ( <i>dd</i> ; 7.2, 1.5)
7	6.39 ( <i>d</i> ; 7.1)	6.38 ( <i>d</i> ; 7.0)	6.37 ( <i>d</i> ; 7.02)	6.30 ( <i>d</i> ; 7.2)
11 $\alpha$	2.03 ( <i>td</i> ; 13.4, 7.0)	2.02 ( <i>td</i> ; 13.7, 5.8)	1.95 ( <i>td</i> ; 14.0, 6.4)	1.97 ( <i>td</i> ; 13.6, 7.1)
11 $\beta$	2.27 ( <i>m</i> )	2.26 ( <i>ddd</i> ; 13.7, 4.9, 2.1)	2.21 ( <i>m</i> )	2.20 ( <i>m</i> )
12 $\alpha$	1.85 ( <i>m</i> )	1.87 ( <i>m</i> )	1.76 ( <i>ddd</i> ; 14.0, 6.4, 3.0)	1.76 ( <i>m</i> )
12 $\beta$	1.84 ( <i>m</i> )	1.84 ( <i>m</i> )	1.81 ( <i>td</i> ; 14.0, 5.0)	1.76 ( <i>m</i> )
15 $\alpha$	1.88 ( <i>td</i> ; 13.5, 4.7)	1.81 ( <i>td</i> ; 14.0, 4.1)	1.84 ( <i>m</i> )	1.80 ( <i>td</i> ; 13.4, 4.0)
15 $\beta$	1.66 ( <i>ddd</i> ; 13.5, 5.3, 1.9)	1.65 ( <i>m</i> )	1.73 ( <i>m</i> )	1.57 ( <i>ddd</i> ; 13.4, 4.6, 2.4)
16 $\alpha$	2.27 ( <i>m</i> )	1.46 ( <i>ddd</i> ; 14.0, 4.1, 2.3)	1.65 ( <i>m</i> )	1.50 ( <i>ddd</i> ; 13.4, 4.0, 2.4)
16 $\beta$	1.61 ( <i>m</i> )	1.91 ( <i>td</i> ; 14.0, 4.9)	1.89 ( <i>m</i> )	1.88 ( <i>td</i> ; 13.4, 4.6)
18	1.82 ( <i>d</i> ; 7.4)	1.67 ( <i>d</i> ; 7.2)	1.94 ( <i>dd</i> ; 9.0, 4.3)	1.75 ( <i>m</i> )
19 $\alpha$	2.22 ( <i>dd</i> ; 14.3, 6.5)	2.20 ( <i>dd</i> ; 15.0, 6.4)	2.28 ( <i>dd</i> ; 15.6, 9.0)	2.29 ( <i>m</i> )
19 $\beta$	1.78 ( <i>ddd</i> ; 14.3, 12.9, 7.4)	1.76 ( <i>ddd</i> ; 15.0, 13.1, 7.2)	2.20 ( <i>dd</i> ; 15.6, 4.3)	2.29 ( <i>m</i> )
20	2.66 ( <i>ddq</i> ; 12.9, 6.5, 6.5)	2.50 ( <i>ddq</i> ; 13.1, 6.5, 6.5)		
22 $\alpha$	4.55 ( <i>d</i> ; 3.7)	2.92 ( <i>d</i> ; 15.1)	3.00 ( <i>d</i> ; 14)	2.75 ( <i>d</i> ; 19.2)
22 $\beta$		1.86 ( <i>d</i> ; 15.1)	1.95 ( <i>d</i> ; 14)	2.17 ( <i>d</i> ; 19.2)
23	2.23 ( <i>s</i> )	2.23 ( <i>s</i> )	2.22 ( <i>s</i> )	2.21 ( <i>s</i> )
25	1.52 ( <i>s</i> )	1.51 ( <i>s</i> )	1.48 ( <i>s</i> )	1.46 ( <i>s</i> )
26	1.37 ( <i>s</i> )	1.35 ( <i>s</i> )	1.37 ( <i>s</i> )	1.34 ( <i>s</i> )
27	0.98 ( <i>s</i> )	0.98 ( <i>s</i> )	0.89 ( <i>s</i> )	0.62 ( <i>s</i> )
28	0.87 ( <i>s</i> )	1.02 ( <i>s</i> )	1.13 ( <i>s</i> )	1.28 ( <i>s</i> )
29			1.36 ( <i>s</i> )	
30	1.07 ( <i>d</i> ; 6.49)	1.00 ( <i>s</i> )		1.38 ( <i>s</i> )
3-OH	6.97 ( <i>br s</i> )	6.98 ( <i>br s</i> )	6.97 ( <i>br s</i> )	6.97 ( <i>br s</i> )
20-OH			3.24 ( <i>s</i> )	3.06 ( <i>s</i> )
22-OH	3.66 ( <i>d</i> ; 3.7)			

\* Chemical shifts are reported as ppm ( $\delta$ ) from TMS in CDCl<sub>3</sub>, signal multiplicity and coupling constant (Hz) are in parentheses.



Table 5.  $^{13}\text{C}$  NMR assignments of GS-T-1 (1), GS-T-2 (15), GS-Y1-1 (2) and GS-Y1-2 (45).\*

Carbon	GS-T-1 (1)	GS-T-2 (15)	GS-Y1-1 (2)	GS-Y1-2 (45)
1	119.8	119.8	119.7	119.7
2	178.4	178.4	178.4	178.4
3	146.0	146.0	146.1	146.0
4	117.2	117.1	117.2	117.0
5	127.7	127.7	127.7	127.6
6	133.7	133.6	133.7	133.6
7	118.1	118.1	118.3	117.8
8	168.4	168.7	169.0	168.8
9	42.6	42.7	43.0	42.7
10	164.7	164.7	164.3	164.6
11	34.0	33.8	33.1	33.8
12	29.9	29.9	29.8	28.9
13	40.5	40.6	39.9	39.6
14	44.3	44.6	44.1	44.1
15	28.2	28.5	29.2	28.1
16	29.5	35.5	35.6	36.5
17	44.8	38.2	36.0	34.7
18	45.0	43.5	43.3	43.8
19	32.0	32.0	39.8	34.5
20	40.8	41.8	73.7	72.0
21	213.5	213.6	215.1	216.3
22	76.3	52.5	50.4	47.8
23	10.2	10.2	10.3	10.2
25	39.1	39.0	38.5	38.8
26	21.6	21.5	23.1	21.7
27	20.5	19.7	19.4	16.8
28	25.0	32.5	33.1	34.7
29			29.0	
30	14.7	15.1		30.8

\* Chemical shifts are reported as ppm ( $\delta$ ) from TMS in  $\text{CDCl}_3$ .

#### 1.1.4) Structure elucidation of GS-Y2-1 and GS-Y2-2

GS-Y2-1 and GS-Y2-2 were identical in their molecular formulae,  $C_{28}H_{36}O_5$ , according to MS (Figure 75, page 193, and Figure 84, page 206) and  $^{13}C$  NMR spectra (Figure 77, page 196, and Figure 86, page 209). Their spectroscopic data were also very similar. Both compounds possessed two carbon signals in the  $\delta$  72-76 ppm region, which were defined by DEPT technique (Figure 77, page 196 and Figure 86, page 209), as a methine and a quaternary carbons. The methine carbon was proved to be C-22, according to three-bond correlations between this carbon and H-18 and 3H-28 (Figure 80, page 201-202, and Figure 89, page 214-219). Its quite downfield signals of  $^1H$  ( $\delta$  4.98 or 4.57 ppm) and  $^{13}C$  ( $\delta$  73.8 or 76.7 ppm) indicated a hydroxyl group which showed  $^1H$  signal coupling to the methine proton (Figure 78, page 197, and Figure 87, page 210) as substituting at this position. A geminal hydroxyl group and methyl group was also suggested according to the downfield shift of the quaternary carbon signal ( $\delta$  72.4 or 73.2 ppm) and the methyl proton singlet ( $\delta$  1.40 ppm). The three-bond correlation between the methyl protons and C-19 indicated that the quaternary carbon should be at position 20. Moreover, the methyl protons and H-19 also displayed three-bond correlation to carbonyl carbon at position 21. Therefore, it could be established that the gross structure of GS-Y2-1, as well as GS-Y2-2, were 20,22-dihydroxy derivatives of tingenone (Figure 8).

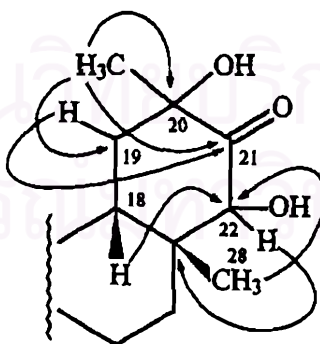


Figure 8. Some important  $^1H$ - $^{13}C$  HMBC long-range correlations in ring E of GS-Y2-1 and GS-Y2-2.

Stereochemistry was the only possible difference between these compounds. Both compounds showed *NOE* correlation between H-22 and 3H-27 (Figure 81 (b), page 204, and Figure 90 (b), page 221). Thus, the same configuration at C-22,  $\alpha$ -H /  $\beta$ -OH, was established. The 20-CH<sub>3</sub> of GS-Y2-1 displayed *NOE* to 3H-28 (Figure 81 (a), page 203) but it was to 3H-27 in GS-Y2-2 (Figure 90 (a), page 220), indicating opposite configurations at C-20 of,  $\alpha$ -OH /  $\beta$ -CH<sub>3</sub> and  $\alpha$ -CH<sub>3</sub> /  $\beta$ -OH, respectively. These *NOEs* were summarized in Figure 9. Therefore, GS-Y2-1 was elucidated as 20,22 $\beta$ -dihydroxy-tingenone (46) and GS-Y2-2 was its 20-epimeric stereoisomer, 20,22 $\beta$ -dihydroxy-20-epi-tingenone (47), both of which were novel structures. Their <sup>1</sup>H and <sup>13</sup>C NMR assignments were shown in Tables 6 and 7 (page 89-90).

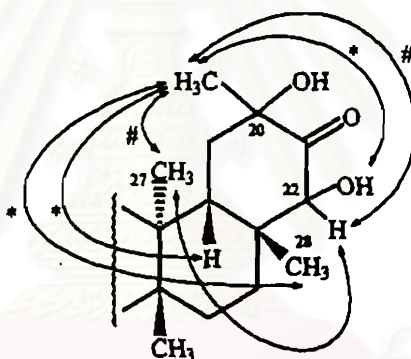
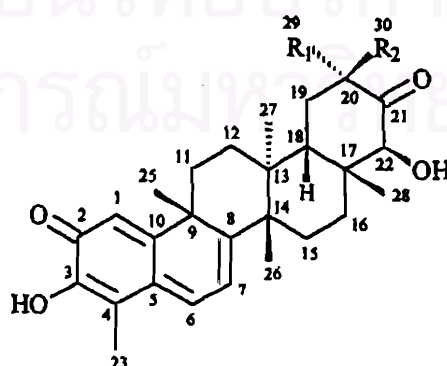


Figure 9. *NOEs* observed in ring E of GS-Y2-1 and GS-Y2-2.

\* found only in GS-Y2-1

# found only in GS-Y2-2



R<sub>1</sub> R<sub>2</sub>

(46) GS-Y2-1 OH CH<sub>3</sub>

(47) GS-Y2-2 CH<sub>3</sub> OH

Conformation of both compounds was the other point of interest. If ring E of GS-Y2-1 exhibited chair conformation, the oxygen atom of 20-OH should be at close proximity to the 3H-27 and caused downfield shift, whereas if it was boat conformation similar to that of GS-Y1-2 just described in previous section, the shielding effect of carbonyl functionality at position 21 would result in the upfield signal. In fact,  $^1\text{H}$  signal of 3H-27 was in normal range ( $\delta$  1.02 ppm). Therefore, semi-chair conformation was suggested and supported by MM2 force field calculation (Figure 10). The influence of both functional groups to 3H-27 were neutralized in this character.

As in GS-Y2-1, 3H-27 signal of GS-Y2-2 was in normal range ( $\delta$  0.92 ppm). Hence, chair conformation of ring E was suggested and neither functional group would significantly affect 3H-27. Most feasible conformation of GS-Y2-2 was also confirmed by MM2 force field calculation (Figure 11).

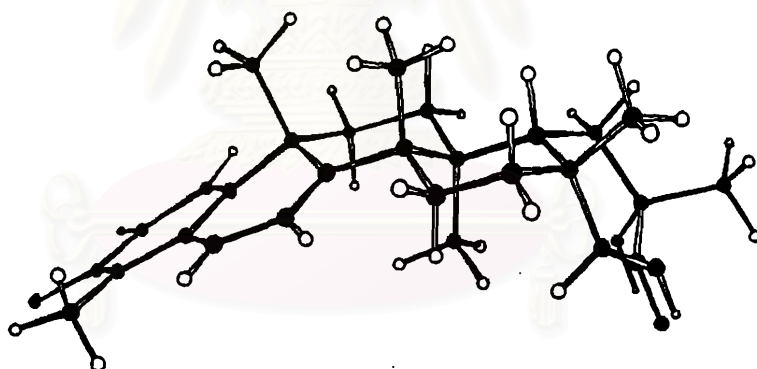


Figure 10. Most stable conformation of GS-Y2-1, calculated by MM2 force field (52.367 kcal/mole).

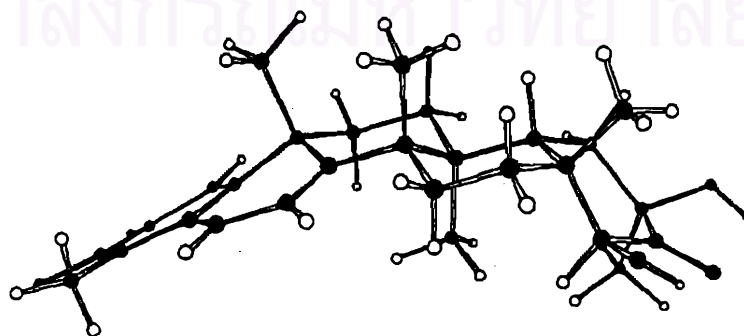


Figure 11. Most stable conformation of GS-Y2-2, calculated by MM2 force field (53.600 kcal/mole).

### 1.1.5) Structure elucidation of GS-Y2-5

GS-Y2-5 was shown to have the same molecular formula,  $C_{28}H_{36}O_4$ , as GS-Y2-1 and GS-Y2-2 by MS (Figure 102, page 235) and  $^{13}C$  NMR spectrum (Figure 104, page 238). Its  $^{13}C$  signals at  $\delta$  75.5, 75.7 and 215.3 ppm were defined by DEPT technique (Figure 104, page 238) as a quaternary, a methine and a quaternary carbonyl carbon, respectively. Analysis of  $^1H$ - $^{13}C$  long-range spectrum (Figure 107, page 241-245) indicated the quaternary carbon to be the C-20 by the evidences of three-bond and two-bond connectivities to H-18 ( $\delta$  2.28 ppm) and H-19 $\beta$  ( $\delta$  2.20 ppm). Its quite downfield signal and a two-bond correlation to a singlet methyl proton signal ( $\delta$  1.41 ppm) suggested that a hydroxyl and methyl groups should be placed at this position. This quaternary carbon and its substituted methyl carbon ( $\delta$  31.5 ppm) showed long-range correlations to a methine proton at  $\delta$  4.33 ppm which further connected to a carbonyl carbon ( $\delta$  215.3 ppm), based on their two-bond correlation. The carbonyl carbon also revealed several long-range correlations to H-16 $\alpha$  ( $\delta$  2.64 ppm), H-18 ( $\delta$  2.28 ppm) and H-28 ( $\delta$  1.44 ppm), therefore, resulting in ring closure as shown in Figure 12.

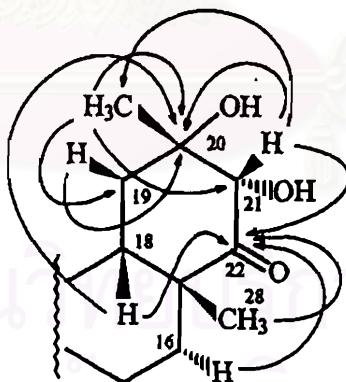
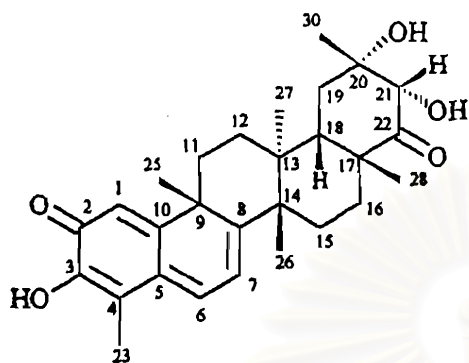


Figure 12.  $^1H$ - $^{13}C$  HMBC long-range correlations of ring E of GS-Y2-5.

Stereochemistry at C-20 and C-21 of GS-Y2-5 were determined by NOE technique (Figure 13, and Figure 108, page 246-247). The 17- $CH_3$ , H-21 and 20- $CH_3$  were demonstrated to have the same  $\beta$ -orientation. Therefore, GS-Y2-5 was assigned the novel structure 3,20 $\alpha$ ,21 $\alpha$ -trihydroxy-D:A-friedo-24,29-dinoroleana-1(10),3,5,7-tetraene-2,22-dione or 20,21 $\alpha$ -dihydroxy-22-oxo-21-desoxo-tingenone (48). Its  $^1H$  and  $^{13}C$  NMR assignments were shown in Tables 6 and 7 (page 89-90).



(48)

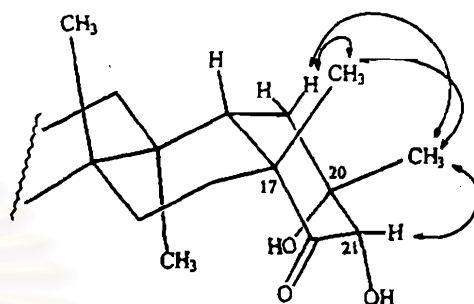


Figure 13. NOEs observation of GS-Y2-5 in part of ring E.

Conformation of ring E of this compound was determined to be chair by the upfield signal of 3H-27 ( $\delta$  0.59 ppm), and result calculated from MM2 force field (Figure 14). However, the strong shielding effect from C=O at position 21 was slightly reduced by the electrostatic effect of 20 $\alpha$ -OH.

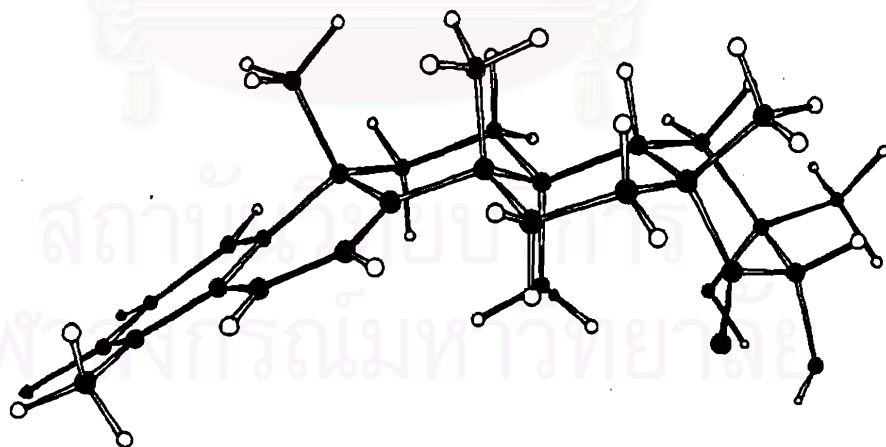


Figure 14. Most stable conformation of GS-Y2-5, calculated by MM2 force field (49.702 kcal/mole).

Table 6. <sup>1</sup>H NMR assignments of GS-Y2-1 (46), GS-Y2-2 (47) and GS-Y2-5 (48).\*

Proton	GS-Y2-1 (46)	GS-Y2-2 (47)	GS-Y2-5 (48)
1	6.54 ( <i>d</i> ; 1.5)	6.54 ( <i>d</i> ; 1.3)	6.51 ( <i>d</i> ; 1.4)
6	7.05 ( <i>dd</i> ; 7.2, 1.5)	7.04 ( <i>dd</i> ; 7.2, 1.3)	7.01 ( <i>dd</i> ; 7.2, 1.4)
7	6.38 ( <i>d</i> ; 7.2)	6.41 ( <i>d</i> ; 7.2)	6.33 ( <i>d</i> ; 7.2)
11 $\alpha$	2.00 ( <i>d</i> ; 13.8, 6.2)	1.92 ( <i>td</i> ; 13.7, 5.2)	1.86 ( <i>td</i> ; 13.7, 5.3)
11 $\beta$	2.22 ( <i>ddd</i> ; 13.8, 5.2, 2.5)	2.21 ( <i>m</i> )	2.14 ( <i>ddd</i> ; 13.7, 4.3, 2.5)
12 $\alpha$	1.81 ( <i>ddd</i> ; 13.8, 6.2, 2.5)	1.74 ( <i>ddd</i> ; 13.7, 5.2, 2.7)	1.79 ( <i>dd</i> ; 13.7, 5.3)
12 $\beta$	1.76 ( <i>td</i> ; 13.8, 5.2)	1.84 ( <i>td</i> ; 13.7, 3.6)	1.71 ( <i>td</i> ; 13.7, 4.3)
15 $\alpha$	1.92 ( <i>dd</i> ; 13.4, 5.5)	1.88 ( <i>m</i> )	1.76 ( <i>m</i> )
15 $\beta$	1.65 ( <i>ddd</i> ; 13.4, 6.3, 2.4)	1.77 ( <i>ddd</i> ; 13.5, 7.1, 3.8)	1.62 ( <i>dd</i> ; 13.3, 5.3)
16 $\alpha$	1.58 ( <i>dd</i> ; 15.6, 6.3)	1.66 ( <i>ddd</i> ; 15.6, 7.9, 7.1)	2.64 ( <i>ddd</i> ; 14.9, 5.7, 1.6)
16 $\beta$	2.35 ( <i>ddd</i> ; 15.6, 5.5, 2.4)	2.34 ( <i>ddd</i> ; 15.6, 7.7, 3.8)	1.52 ( <i>m</i> )
18	1.92 ( <i>dd</i> ; 9.2, 1.8)	2.09 ( <i>dd</i> ; 7.6, 6.6)	2.28 ( <i>dd</i> ; 10.1, 1.8)
19 $\alpha$	2.28 ( <i>dd</i> ; 16.2, 1.8)	2.18 ( <i>dd</i> ; 15.2, 6.6)	2.26 ( <i>dd</i> ; 12.2, 1.8)
19 $\beta$	2.05 ( <i>dd</i> ; 16.2, 9.2)	2.23 ( <i>dd</i> ; 15.2, 7.6)	2.20 ( <i>dd</i> ; 12.2, 10.1)
21			4.33 ( <i>d</i> ; 2.8)
22	4.98 ( <i>d</i> ; 4.4)	4.57 ( <i>d</i> ; 4.7)	
23	2.23 ( <i>s</i> )	2.22 ( <i>s</i> )	2.21 ( <i>s</i> )
25	1.48 ( <i>s</i> )	1.47 ( <i>s</i> )	1.43 ( <i>s</i> )
26	1.35 ( <i>s</i> )	1.39 ( <i>s</i> )	1.28 ( <i>s</i> )
27	1.02 ( <i>s</i> )	0.92 ( <i>s</i> )	0.59 ( <i>s</i> )
28	0.86 ( <i>s</i> )	0.99 ( <i>s</i> )	1.44 ( <i>s</i> )
29		1.40 ( <i>s</i> )	
30	1.40 ( <i>s</i> )		1.41 ( <i>s</i> )
3-OH	6.96 ( <i>br s</i> )	6.98 ( <i>br s</i> )	6.96 ( <i>br s</i> )
20-OH		2.98 ( <i>br s</i> )	
21-OH			3.89 ( <i>d</i> ; 2.8)
22-OH	3.40 ( <i>d</i> ; 4.4)	3.40 ( <i>d</i> ; 4.7)	

\* Chemical shifts are reported as ppm ( $\delta$ ) from TMS in CDCl<sub>3</sub>, signal multiplicity and coupling constant (Hz) are in parentheses.

Table 7.  $^{13}\text{C}$  NMR assignments of GS-Y2-1 (46), GS-Y2-2 (47) and GS-Y2-5 (48). \*

Carbon	GS-Y2-1 (46)	GS-Y2-2 (47)	GS-Y2-5 (48)
1	119.6	119.6	119.5
2	178.4	178.4	178.4
3	146.0	146.1	146.0
4	117.2	117.2	117.0
5	127.5	127.7	127.5
6	134.0	133.7	133.8
7	118.0	118.6	118.2
8	169.4	169.0	168.7
9	42.8	43.0	42.8
10	164.7	164.1	164.2
11	33.8	33.0	33.2
12	29.6	29.7	29.4
13	39.6	39.8	39.3
14	44.2	43.7	44.5
15	28.7	29.5	29.0
16	29.4	29.7	27.9
17	42.4	40.2	45.0
18	44.8	43.1	49.6
19	35.1	35.1	31.0
20	72.4	73.2	75.5
21	211.5	215.3	75.7
22	73.8	76.7	215.3
23	10.3	10.3	10.2
25	38.7	38.1	37.4
26	22.1	24.1	21.9
27	19.3	19.8	18.5
28	25.4	26.1	31.6
29		28.7	
30	26.1		31.5

\* Chemical shifts are reported as ppm ( $\delta$ ) from TMS in  $\text{CDCl}_3$ .



### 1.1.6) Structure elucidation of GS-Y2-4 and GS-Y2-6

GS-Y2-4 and GS-Y2-6 were determined to possess the same molecular formulae of  $C_{28}H_{34}O_4$  by MS (Figure 93, page 223, Figure 111, page 249) and  $^{13}C$  NMR spectra (Figure 95, page 226, and Figure 113, page 252). Their spectroscopic data were very similar. In  $^{13}C$  NMR and DEPT spectra of both compounds, there were a quaternary carbon at  $\delta$  74 ppm and two carbonyl quaternary carbons in the range of  $\delta$  195-200 ppm. Based on their  $^1H$ - $^{13}C$  long-range spectra (Figure 98, page 229-232, and Figure 116, page 255-258), the quaternary carbon should be the C-20, of which three-bond correlation to H-18 and two-bond correlations to H-19 $\alpha$  and H-19 $\beta$  were detected. A methyl group should be placed at this position, according to the singlet methyl signal and its two-bond correlation with this carbon. Moreover, a hydroxyl substitution was also suggested, causing downfield shift of the quaternary carbon signal.

The two carbonyl quaternary carbons at  $\delta$  199-200 and 195-196 ppm were proved to be the C-21 and C-22, respectively, by their  $^1H$ - $^{13}C$  long-range correlation data. The more downfield carbonyl carbon showed three-bond correlations with H-19 $\alpha$  and the methyl proton on C-20. The other one displayed three-bond connectivities to H-16, H-18 and 3H-28. These evidences proved that GS-Y2-4, as well as GS-Y2-6, were the 20-hydroxy-22-oxo derivatives of tingenone (Figure 15).

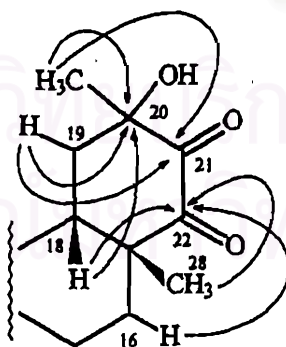


Figure 15.  $^1H$ - $^{13}C$  HMBC long-range correlations of ring E of GS-Y2-4 and GS-Y2-6.

Configuration at C-20 was the only difference between these two compounds. The *NOE* correlation was observed between 20-CH<sub>3</sub> and 17-CH<sub>3</sub> for GS-Y2-4, while in GS-Y2-6, 20-CH<sub>3</sub> displayed *NOE* to 13-CH<sub>3</sub> (Figure 99, page 233, and Figure 117, page 259, or summarized in Figure 16). Therefore, GS-Y2-4 was elucidated as 20-hydroxy-22-oxo-tingenone (49), and GS-Y2-6 was its 20-epimeric stereoisomer, 20-hydroxy-22-oxo-20-epi-tingenone (50), both of which were novel structures. Their <sup>1</sup>H and <sup>13</sup>C NMR assignments were shown in Tables 8 and 9 (page 96-97).

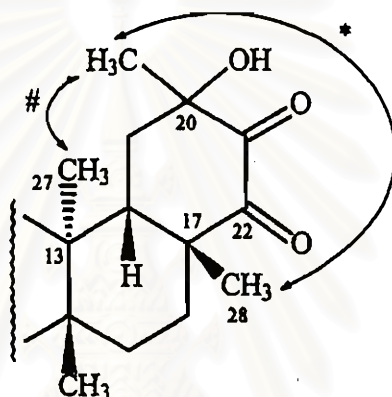
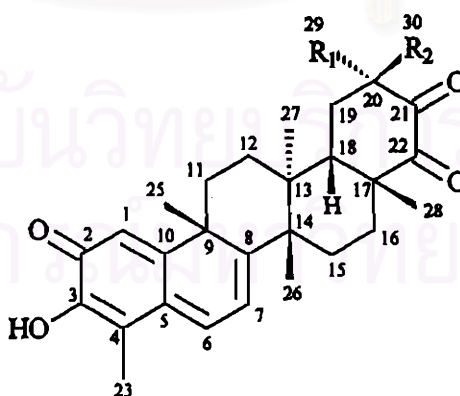


Figure 16. *NOEs* observation of ring E of GS-Y2-4 and GS-Y2-6.

\* found only in GS-Y2-4

# found only in GS-Y2-6



	R <sub>1</sub>	R <sub>2</sub>
(49) GS-Y2-4	OH	CH <sub>3</sub>
(50) GS-Y2-6	CH <sub>3</sub>	OH

Ring E conformation of both compounds were semi-chair, according to the results calculated by MM2 force field (Figures 17 and 18). Thus, anisotropic effects of C=O at position 21 and 22 would result 3H-27 displaying its signal at very upfield regions ( $\delta$  0.58 ppm for GS-Y2-4 and 0.42 ppm for GS-Y2-6). Electrostatic effect from oxygen atom of the 20 $\alpha$ -OH of GS-Y2-4 caused it to be slightly more downfield.

According to the same semi-chair conformation, the 20-OH of each compound would be closer to either H-19 $\alpha$  or H-19 $\beta$ , resulting in more downfield shift of one of them. In GS-Y2-4, signal of H-19 $\alpha$  ( $\delta$  2.47 ppm) was more downfield than that of H-19 $\beta$  ( $\delta$  2.40 ppm), while GS-Y2-6 displayed the opposite result ( $\delta_{\text{H-19}\alpha}$  2.35 ppm and  $\delta_{\text{H-19}\beta}$  2.56 ppm). This careful comparison between the two compounds supported both configuration and conformation.

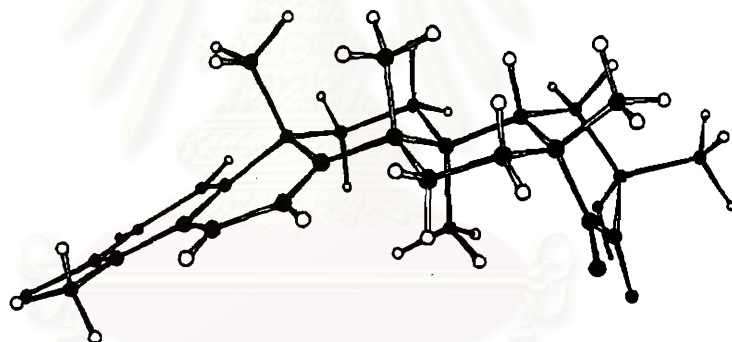


Figure 17. Most stable conformation of GS-Y2-4, calculated by MM2 force field (55.539 kcal/mole).

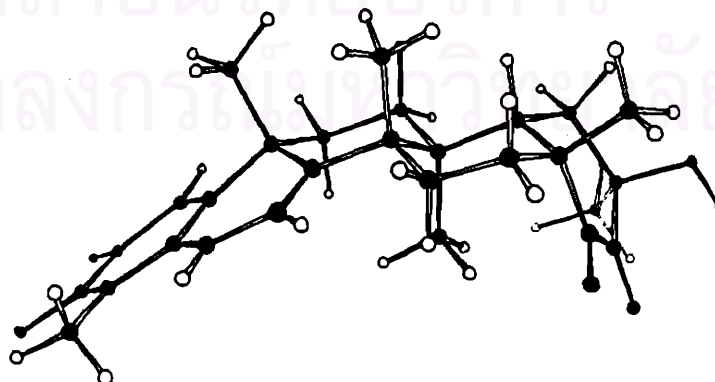


Figure 18. Most stable conformation of GS-Y2-6, calculated by MM2 force field (58.466 kcal/mole).

### 1.1.7) Structure elucidation of GS-Y3-2

Similar to GS-Y2-4 and GS-Y2-6, the molecular formula of GS-Y3-2 was shown to be  $C_{28}H_{34}O_4$  by MS (Figure 120, page 261) and  $^{13}C$  NMR spectrum (Figure 122, page 264). There were a quaternary carbon and two carbonyl quaternary  $^{13}C$  signal appeared at  $\delta$  82.7, 209.4 and 212.9 ppm, respectively. The slightly more upfield carbonyl carbon signal was demonstrated to be the C-20 according to its long-range correlations to H-18 ( $\delta$  2.27 ppm), H-19 $\alpha$  ( $\delta$  2.97 ppm) and H-19 $\beta$  ( $\delta$  3.09 ppm). The other carbonyl carbon, displaying three-bond correlations to H-18 ( $\delta$  2.27 ppm) and 3H-28 ( $\delta$  1.48 ppm), was assigned to be the C-22. The quaternary carbon, substituted with a methyl group owing to their two-bond correlations, was unequivocally the C-21 according to its three-bond connectivity to H-19 $\alpha$ , and also from its substituted methyl proton ( $\delta$  1.57 ppm) to both carbonyl carbons. A hydroxyl group was suggested as substituting on this carbon, thus causing the downfield signal. All of these correlations were shown in Figure 125 (page 267-269) and summarized in Figure 19.

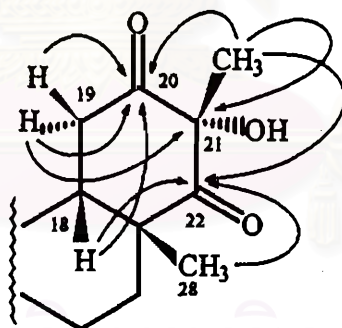


Figure 19.  $^1H$ - $^{13}C$  HMBC long-range correlations of ring E of GS-Y3-2.

The configuration of the only chiral carbon of ring E at C-21 was defined as  $\alpha$ -OH /  $\beta$ -CH $_3$  by the *NOEs* observed among the 21 $\beta$ -CH $_3$ , H-19 $\beta$  and 3H-28 (Figure 20, and Figure 126, page 270), which indicated ring E as exhibiting chair conformation. The result calculated from MM2 force field (Figure 21) also confirm this suggestion. The very upfield signal of 3H-27 at  $\delta$  0.29 ppm was strongly influenced by the anisotropic effect of both carbonyl groups, while 21 $\alpha$ -OH did not affect it in this conformation.

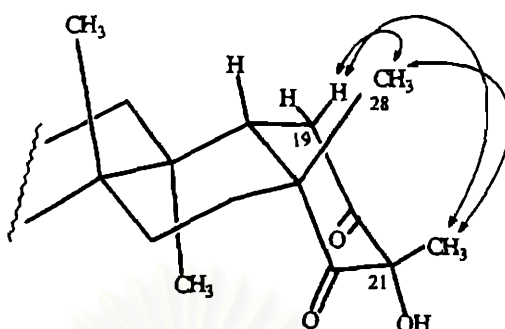
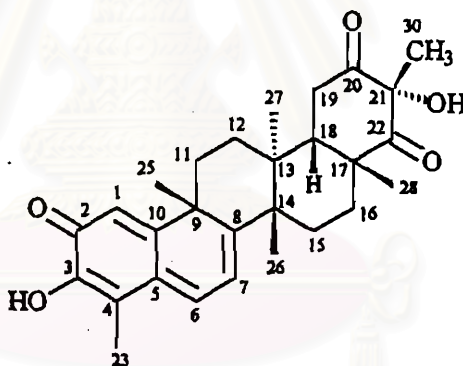


Figure 20. NOEs observation in ring E of GS-Y3-2.

These NMR evidences indicated that GS-Y3-2 was 21 $\alpha$ -hydroxy-20,22-dioxo-30(20 $\rightarrow$ 21)*abeo*-21-desoxo-tingenone (51), a quinone-methide triterpene with novel carbon skeleton. Its  $^1\text{H}$  and  $^{13}\text{C}$  NMR assignments were shown in Tables 8 and 9 (page 96-97).



(51)

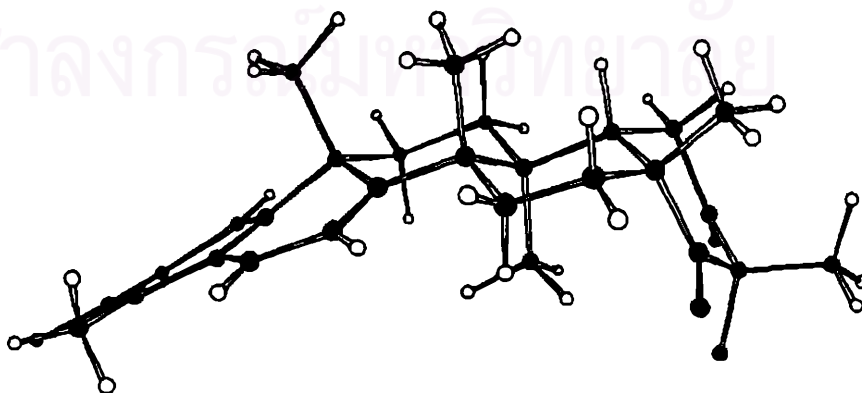


Figure 21. Most stable conformation of GS-Y3-2, calculated by MM2 force field (53.941 kcal/mole).

Table 8. <sup>1</sup>H NMR assignments of GS-Y2-4 (49), GS-Y2-6 (50) and GS-Y3-2 (51).\*

Proton	GS-Y2-4 (49)	GS-Y2-6 (50)	GS-Y3-2 (51)
1	6.51 ( <i>d</i> , <i>J</i> = 1.4)	6.50 ( <i>d</i> , <i>J</i> = 1.4)	6.48 ( <i>d</i> ; 1.4)
6	6.99 ( <i>dd</i> , <i>J</i> = 7.2, 1.4)	7.00 ( <i>dd</i> , <i>J</i> = 7.1, 1.4)	6.97 ( <i>dd</i> ; 7.2, 1.4)
7	6.26 ( <i>d</i> , <i>J</i> = 7.2)	6.28 ( <i>d</i> , <i>J</i> = 7.1)	6.27 ( <i>d</i> ; 7.2)
11 $\alpha$	1.91 ( <i>td</i> , <i>J</i> = 13.6, 5.3)	1.87 ( <i>m</i> )	1.80 ( <i>td</i> ; 13.4, 4.3)
11 $\beta$	2.22 ( <i>dt</i> , <i>J</i> = 13.6, 4.2)	2.26 ( <i>m</i> )	2.20 ( <i>m</i> )
12 $\alpha$	1.87 ( <i>m</i> )	1.71 ( <i>dt</i> , <i>J</i> = 7.9, 2.2)	1.76 ( <i>m</i> )
12 $\beta$	1.82 ( <i>dt</i> , <i>J</i> = 13.6, 4.2)	1.87 ( <i>m</i> )	1.85 ( <i>td</i> , 14.3, 4.0)
15 $\alpha$	1.64 ( <i>m</i> )	1.67 ( <i>m</i> )	1.55 ( <i>td</i> ; 14.3, 4.3)
15 $\beta$	1.58 ( <i>ddd</i> , <i>J</i> = 12.1, 5.2, 2.7)	1.61 ( <i>m</i> )	1.58 ( <i>ddd</i> ; 14.3, 5.2, 2.1)
16 $\alpha$	2.65 ( <i>dt</i> , <i>J</i> = 13.3, 2.7)	2.64 ( <i>dt</i> , <i>J</i> = 12.8, 3.0)	2.85 ( <i>ddd</i> ; 14.3, 4.3, 2.1)
16 $\beta$	1.75 ( <i>td</i> , <i>J</i> = 13.3, 5.2)	1.62 ( <i>m</i> )	1.65 ( <i>td</i> ; 14.3, 5.2)
18	2.12 ( <i>dd</i> , <i>J</i> = 6.7, 1.7)	2.23 ( <i>d</i> , <i>J</i> = 9.2)	2.27 ( <i>dd</i> ; 6.7, 2.1)
19 $\alpha$	2.47 ( <i>dd</i> , <i>J</i> = 16.6, 1.7)	2.35 ( <i>d</i> , <i>J</i> = 16.1)	2.97 ( <i>dd</i> ; 16.5, 2.1)
19 $\beta$	2.40 ( <i>dd</i> , <i>J</i> = 16.6, 6.7)	2.56 ( <i>dd</i> , <i>J</i> = 16.1, 9.2)	3.09 ( <i>dd</i> ; 16.5, 6.7)
23	2.20 ( <i>s</i> )	2.20 ( <i>s</i> )	2.19 ( <i>s</i> )
25	1.45 ( <i>s</i> )	1.47 ( <i>s</i> )	1.45 ( <i>s</i> )
26	1.34 ( <i>s</i> )	1.35 ( <i>s</i> )	1.35 ( <i>s</i> )
27	0.58 ( <i>s</i> )	0.42 ( <i>s</i> )	0.29 ( <i>s</i> )
28	1.32 ( <i>s</i> )	1.50 ( <i>s</i> )	1.48 ( <i>s</i> )
29		1.56 ( <i>s</i> )	
30	1.48 ( <i>s</i> )		1.57 ( <i>s</i> )
3-OH	6.96 ( <i>br s</i> )	6.94 ( <i>br s</i> )	6.93 ( <i>br s</i> )
20-OH	2.84 ( <i>br s</i> )		

\* Chemical shifts are reported as ppm ( $\delta$ ) from TMS in CDCl<sub>3</sub>, signal multiplicity and coupling constant (Hz) are in parentheses.

สถาบันวิทยบริการ  
จุฬาลงกรณ์มหาวิทยาลัย

Table 9.  $^{13}\text{C}$  NMR assignments of GS-Y2-4 (49), GS-Y2-6 (50) and GS-Y3-2 (51).\*

Carbon	GS-Y2-4 (49)	GS-Y2-6 (50)	GS-Y3-2 (51)
1	119.7	119.8	119.8
2	178.4	178.4	178.4
3	146.1	146.1	146.1
4	117.1	117.1	117.0
5	127.7	127.8	127.9
6	133.5	133.5	133.2
7	118.4	118.6	118.7
8	167.3	166.8	166.3
9	42.6	42.5	42.5
10	164.0	164.0	163.8
11	33.6	33.6	33.2
12	28.1	28.7	28.8
13	39.9	40.7	40.1
14	43.8	43.8	43.9
15	28.8	28.8	28.6
16	28.6	28.6	29.3
17	48.6	48.7	46.0
18	44.6	44.3	45.5
19	31.9	33.4	35.0
20	74.3	74.5	209.4
21	199.2	200.1	82.7
22	196.8	195.6	212.9
23	10.2	10.3	10.2
25	37.8	38.1	37.9
26	21.9	22.0	21.6
27	17.0	18.2	17.6
28	28.0	28.0	29.3
29		27.9	
30	31.1		29.6

\* Chemical shifts are reported as ppm ( $\delta$ ) from TMS in  $\text{CDCl}_3$ .

### 1.1.8) Structure elucidation of GS-Y0-2

Compound GS-Y0-2 displayed one carbon signal in  $^{13}\text{C}$  NMR spectrum (Figure 54, page 167) less than all other compounds. Thus, the molecular ion at  $m/z$  422 in MS (Figure 52, page 164) corresponded to the molecular formula of  $\text{C}_{27}\text{H}_{34}\text{O}_4$ . Besides those of the main structure, there were three carbon signals at  $\delta$  30.1, 205.5 and 206.5 ppm demonstrated by DEPT spectra (Figure 54, page 167) as a methyl, a methine carbonyl and a quaternary carbonyl carbons, respectively. These carbons made the closure of ring E impossible and, hence, *seco* character was implied. The quaternary carbonyl carbon signal displayed long-range correlations to those of the methyl protons ( $\delta$  2.27 ppm), H-19 $\alpha$  ( $\delta$  2.67 ppm) and H-19 $\beta$  ( $\delta$  2.81 ppm). Therefore, an acetyl group should connect to C-19. The methine carbonyl carbon should directly connect to the main structure at C-17, according to its three-bond connectivities to H-16 $\beta$  ( $\delta$  1.71 ppm), H-18 ( $\delta$  2.81 ppm) and 3H-28 ( $\delta$  1.00 ppm), as an formyl side chain. These correlations were shown in HMBC spectrum (Figure 57 page 170-172), and summarized in figure 22.

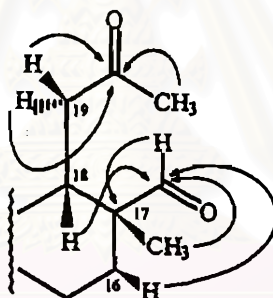
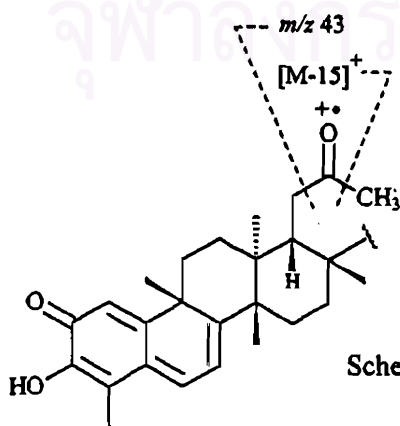


Figure 22.  $^1\text{H}$ - $^{13}\text{C}$  HMBC long-range correlations of ring E of GS-Y0-2.

The mass fragment of  $m/z$  43 was different from those of compounds with closed ring E (Scheme 19). However, it supported the existence of acyl side chain.



Scheme 20. Fragmentation of mass fragments

$m/z$  [M-15] $^+$  and 43 of GS-Y0-2 and GS-Y4-1.



The most stable conformation of both side chains, analyzed by *NOEs* observation (Figure 58, page 173-174), was shown in Figure 23. It was also supported by MM2 calculation (Figure 24). Hence, the upfield signals of H-12 $\alpha$  ( $\delta$  0.96 ppm) and 3H-27 ( $\delta$  0.48 ppm) resulted from the anisotropic effects of C=O at position 20 and 22, respectively.

Based on these evidences, GS-Y0-2 was elucidated as 20-oxo-21-nor-20,21-*seco*-tingen-22-al (52), a quinone-methide triterpene with novel carbon skeleton. Its  $^1\text{H}$  and  $^{13}\text{C}$  NMR assignments were shown in Tables 10 and 11 (page 102-103).

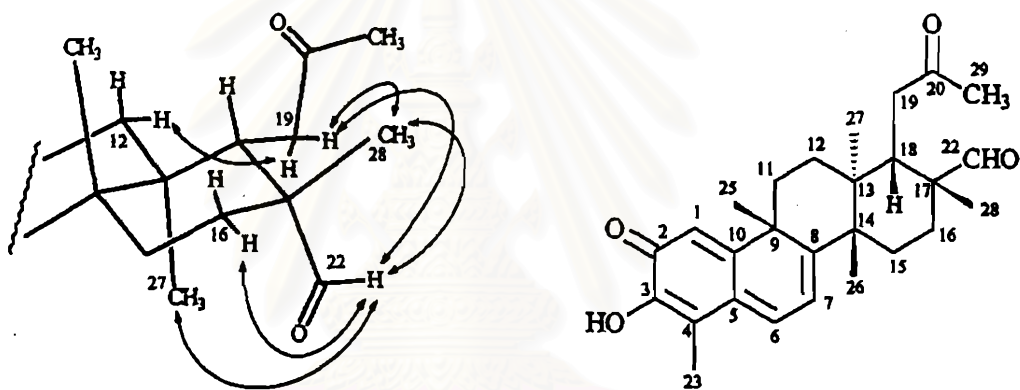


Figure 23. *NOEs* observation in ring E of GS-Y0-2.

(52)

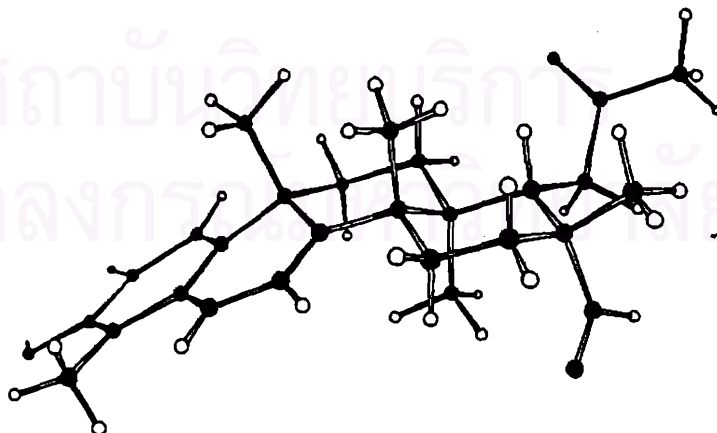


Figure 24. Most stable conformation of GS-Y0-2, calculated by MM2 force field (46.740 kcal/mole).

### 1.1.9) Structure elucidation of GS-Y4-1

The molecular formula of GS-Y4-1 was determined as  $C_{28}H_{36}O_5$  from its MS (Figure 129, page 272) and  $^{13}C$  NMR spectrum (Figure 131, page 275). Its carbon signals besides those of the main structure, at  $\delta$  30.1, 40.5, 176.8 and 206.9 ppm were analyzed by DEPT technique (Figure 131, page 275) as a methyl, a methylene and two quaternary carbonyl carbons, respectively. The closure ring E, therefore, could not accommodate these carbons and similar to GS-Y0-2, a *seco*-ring was suggested. The carbonyl signal at  $\delta$  206.9 ppm showed long-range correlations to the methyl proton signals ( $\delta$  2.23 ppm), H-19 $\alpha$  ( $\delta$  2.50 ppm) and H-19 $\beta$  ( $\delta$  2.31 ppm), thus an acetyl group should connect to the C-19. Another side chain at C-17 appeared to be a methylene-carboxyl functionality, judging from the  $^1H$ - $^{13}C$  long-range correlations from the carboxyl carbon ( $\delta$  176.8 ppm) to both methylene protons ( $\delta$  2.11 and 2.56 ppm), and from the methylene carbon ( $\delta$  40.5 ppm) to H-18 ( $\delta$  2.52 ppm) and 3H-28 ( $\delta$  1.02 ppm). These  $^1H$ - $^{13}C$  long-range correlations were shown in HMBC spectrum (Figure 134, page 278-280), and summarized in Figure 25. Broad absorption band at  $3300$ - $2800$   $cm^{-1}$  in the IR spectrum (Figure 128, page 271) also confirmed the terminal carboxylic acid.

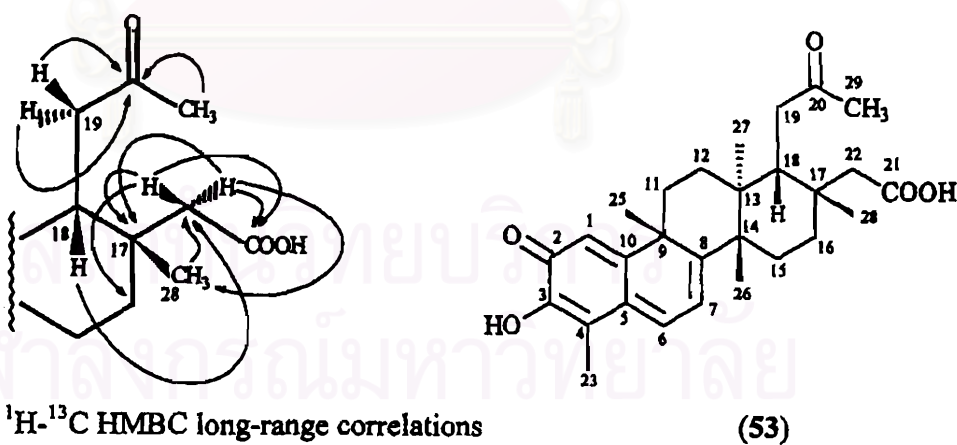


Figure 25.  $^1H$ - $^{13}C$  HMBC long-range correlations of ring E of GS-Y4-1.

(53)

The most stable conformation calculated by MM2 force field was shown in Figure 26. It was supported by the result from NOESY experiment demonstrated in Figure 27, and Figure 135 (page 281). In this conformation, the shielding effect of C=O at position 20 would cause H-12 $\alpha$  to display very upfield signal ( $\delta$  0.94 ppm).

From these spectroscopic evidences, GS-Y4-1 was elucidated as 20-oxo-20,21-*seco*-tingen-21-oic acid (53), a quinone-methide triterpene with novel carbon skeleton. Its  $^1\text{H}$  and  $^{13}\text{C}$  NMR assignments were shown in Tables 10 and 11 (page 102-103).

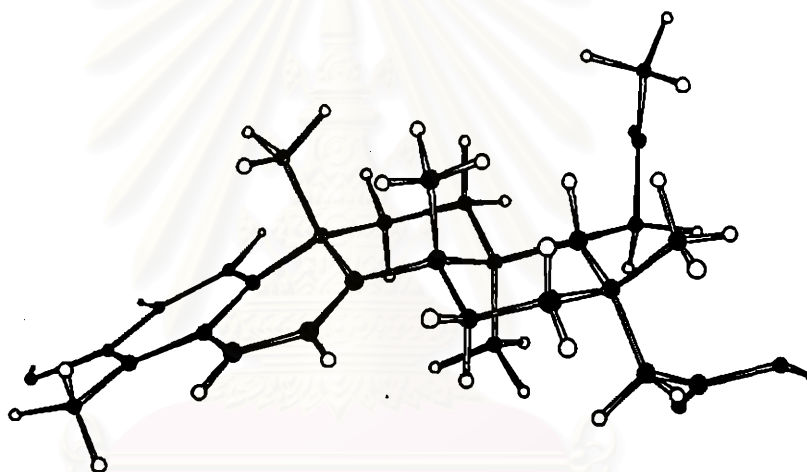


Figure 26. Most stable conformation of GS-Y4-1, calculated by MM2 force field (46.313 kcal/mole).

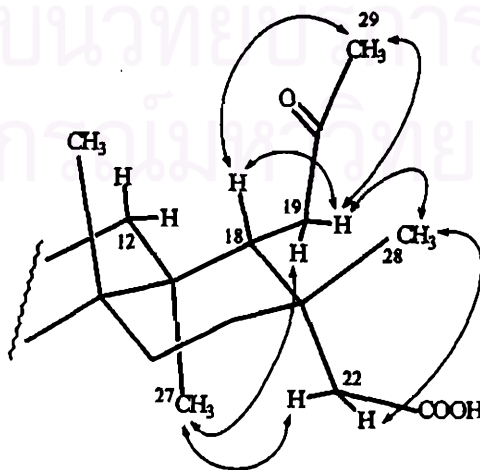


Figure 27. NOEs observation in ring E of GS-Y4-1.

Table 10. <sup>1</sup>H NMR assignments of GS-Y0-2 (52) and GS-Y4-1 (53).\*

Proton	GS-Y0-2 (52)	GS-Y4-1 (53)
1	6.48 ( <i>d</i> ; 1.5)	6.50 ( <i>d</i> ; 1.2)
6	7.01 ( <i>dd</i> ; 7.0, 1.5)	7.04 ( <i>dd</i> ; 7.0, 1.2)
7	6.28 ( <i>d</i> ; 7.0)	6.32 ( <i>d</i> ; 7.0)
11 $\alpha$	1.84 ( <i>m</i> )	1.95 ( <i>td</i> ; 13.4, 5.9)
11 $\beta$	2.15 ( <i>dd</i> ; 8.5, 2.1)	2.17 ( <i>m</i> )
12 $\alpha$	0.96 ( <i>dd</i> ; 8.5, 2.1)	0.94 ( <i>dd</i> ; 13.4, 5.9)
12 $\beta$	1.84 ( <i>m</i> )	1.79 ( <i>td</i> ; 13.4, 6.0)
15 $\alpha$	1.71 ( <i>m</i> )	1.85 ( <i>td</i> ; 13.5, 3.7)
15 $\beta$	1.60 ( <i>m</i> )	1.58 ( <i>br d</i> ; 13.5)
16 $\alpha$	2.31 ( <i>dd</i> ; 10.1, 2.1)	2.15 ( <i>m</i> )
16 $\beta$	1.71 ( <i>m</i> )	1.75 ( <i>td</i> ; 13.5, 4.3)
18	2.81 ( <i>dd</i> ; 7.6, 2.2)	2.52 ( <i>m</i> )
19 $\alpha$	2.67 ( <i>dd</i> ; 19.3, 7.6)	2.50 ( <i>m</i> )
19 $\beta$	2.81 ( <i>dd</i> ; 19.3, 2.2)	2.31 ( <i>d</i> ; 17.4)
22	9.71 ( <i>s</i> )	
22 $\alpha$		2.56 ( <i>d</i> ; 12.5)
22 $\beta$		2.11 ( <i>d</i> ; 12.5)
23	2.20 ( <i>s</i> )	2.23 ( <i>s</i> )
25	1.44 ( <i>s</i> )	1.46 ( <i>s</i> )
26	1.44 ( <i>s</i> )	1.44 ( <i>s</i> )
27	0.48 ( <i>s</i> )	0.58 ( <i>s</i> )
28	1.00 ( <i>s</i> )	1.02 ( <i>s</i> )
29	2.27 ( <i>s</i> )	2.23 ( <i>s</i> )
3-OH	6.95 ( <i>br s</i> )	

\* Chemical shifts are reported as ppm ( $\delta$ ) from TMS in CDCl<sub>3</sub>, signal multiplicity and coupling constant (Hz) are in parentheses.

สถาบันวิทยบริการ  
จุฬาลงกรณ์มหาวิทยาลัย

Table 11.  $^{13}\text{C}$  NMR assignments of GS-Y0-2 (52) and GS-Y4-1 (53).\*

Carbon	GS-Y0-2 (52)	GS-Y4-1 (53)
1	119.7	119.8
2	178.4	178.4
3	146.0	146.1
4	117.1	117.5
5	127.7	127.6
6	133.6	134.0
7	118.0	117.6
8	167.7	169.0
9	42.8	42.8
10	164.2	164.9
11	33.8	33.8
12	28.7	29.4
13	40.6	40.8
14	43.7	44.0
15	29.1	28.4
16	28.4	32.2
17	47.3	35.8
18	42.6	43.4
19	39.3	41.1
20	206.5	206.9
21		176.8
22	205.5	40.5
23	10.2	10.3
25	38.2	39.2
26	22.0	21.7
27	16.5	15.7
28	24.7	28.8
29	30.1	30.1

\* Chemical shifts are reported as ppm ( $\delta$ ) from TMS in  $\text{CDCl}_3$ .

## 1.2) Structure elucidation of acid-rearranged compounds

According to the mechanism proposed in reference [48,65], these acid-rearranged compounds, GS-T-1-ACID, GS-T-2-ACID and GS-Y1-1-ACID, should possess the phenolic-(9→8)-D:A-*friedo*-24-noroleananes skeleton. Based on spectroscopic data, their UV (Figures 136, 139 and 142, pages 282, 285 and 288), IR spectra (Figures 137, 140 and 143, pages 282, 285 and 288) and  $^1\text{H}$  NMR signals in the downfield region (Figures 138,141 and 144, pages 283, 286 and 289) were similar. The UV absorption at  $\lambda_{\text{max}}$  306-307 nm supported the diallyl-phenolic chromophore. The observed single carbonyl band in IR spectra suggested the reaction did not involve the C=O at position 21 of the starting compounds. In  $^1\text{H}$  NMR, the singlet signals at  $\delta$  6.71-6.72 ppm should be that of H-1, while the signals of H-6 and H-7 which appeared as doublets coupling to each other could not be clearly assigned at either 6.44-6.46 or 6.31 ppm. Also the assignments of two broad singlets of hydroxyl groups at C-2 and C-3, might be interchangeable. Comparison to their substrates, revealed the 2H-11 signals to be missing from their usual chemical shifts, while there was an additional doublet signal at  $\delta$  5.54-5.58 ppm which coupled to that of 2H-12.. This downfield signal was suggested to be the lone olefinic proton at C-11, resulting from the rearrangement reaction. All other  $^1\text{H}$  signals were comparable to the substrates. Therefore, the acid-rearranged compounds GS-T-1-ACID, GS-T-2-ACID and GS-Y1-1-ACID, were elucidated as 20 $\beta$ -hydroxy-isotingenone III (54), isotingenone III (55) and 20-hydroxy-20-epi-isotingenone III (56), respectively.

Isotingenone III (55) has been previously found from *Maytenus ilicifolia* Mart. ex Reiss.<sup>51</sup> and *M. ebenifolia* Reiss.<sup>107</sup> and reported as an acid-rearranged product of tingenone<sup>131</sup>. However, this was the first report of the other two compounds.

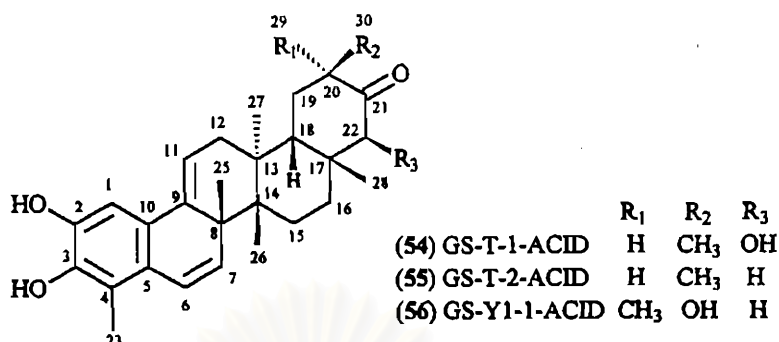


Table 12. <sup>1</sup>H NMR assignments of GS-T-1-ACID (54), GS-T-2-ACID (55) and GS-Y1-1-ACID (56).\*

Proton	GS-T-1-ACID (54)	GS-T-2-ACID (55)	GS-Y1-1-ACID (56)
1	6.72 ( <i>s</i> )	6.72 ( <i>s</i> )	6.71 ( <i>s</i> )
6 <sup>†</sup>	6.46 ( <i>d</i> ; 9.9)	6.46 ( <i>d</i> ; 10.1)	6.44 ( <i>d</i> ; 9.5)
7 <sup>†</sup>	6.31 ( <i>d</i> ; 9.9)	6.31 ( <i>d</i> ; 10.1)	6.31 ( <i>d</i> ; 9.5)
11	5.57 ( <i>d</i> ; 6.7)	5.58 ( <i>d</i> ; 6.1)	5.54 ( <i>d</i> ; 6.1)
12 $\alpha$	2.16 ( <i>dd</i> ; 17.4, 6.7)	2.21 ( <i>dd</i> ; 17.1, 6.1)	2.08 ( <i>m</i> )
12 $\beta$	2.12 ( <i>m</i> )	1.89 ( <i>d</i> ; 17.1)	1.86 ( <i>d</i> ; 16.8)
15 $\alpha$	2.13 ( <i>m</i> )	2.06 ( <i>td</i> ; 13.9, 3.7)	2.06 ( <i>m</i> )
15 $\beta$	1.43 ( <i>dt</i> ; 13.1, 3.5)	1.42 ( <i>dt</i> ; 13.9, 3.7)	1.51 ( <i>dt</i> ; 14.3, 4.1)
16 $\alpha$	2.13 ( <i>m</i> )	1.35 ( <i>dt</i> ; 13.9, 3.7)	1.44 ( <i>dt</i> ; 13.6, 4.1)
16 $\beta$	1.51 ( <i>td</i> ; 15.0, 3.5)	1.80 ( <i>td</i> ; 13.9, 3.7)	1.78 ( <i>td</i> ; 13.6, 4.1)
18	1.92 ( <i>d</i> ; 7.4)	1.77 ( <i>d</i> ; 7.0)	2.03 ( <i>m</i> )
19 $\alpha$	2.06 ( <i>dd</i> ; 14.8, 6.8)	2.07 ( <i>dd</i> ; 14.3, 6.3)	2.31 ( <i>dd</i> ; 15.9, 9.5)
19 $\beta$	1.76 ( <i>ddd</i> ; 14.8, 12.6, 7.4)	1.74 ( <i>ddd</i> ; 14.3, 12.6, 7.0)	2.14 ( <i>dd</i> ; 15.9, 2.1)
20	2.71 ( <i>ddq</i> ; 12.6, 6.8, 6.8)	2.56 ( <i>ddq</i> ; 12.6, 6.3, 6.3)	
22 $\alpha$	4.60 ( <i>s</i> )	2.99 ( <i>d</i> ; 13.6)	3.08 ( <i>d</i> ; 14.1)
22 $\beta$		1.79 ( <i>d</i> ; 13.6)	1.93 ( <i>d</i> ; 14.1)
23	2.22 ( <i>s</i> )	2.22 ( <i>s</i> )	2.21 ( <i>s</i> )
25	1.07 ( <i>s</i> )	1.06 ( <i>s</i> )	1.06 ( <i>s</i> )
26	1.32 ( <i>s</i> )	1.32 ( <i>s</i> )	1.21 ( <i>s</i> )
27	1.04 ( <i>s</i> )	1.03 ( <i>s</i> )	1.05 ( <i>s</i> )
28	0.81 ( <i>s</i> )	0.96 ( <i>s</i> )	1.04 ( <i>s</i> )
29			1.40 ( <i>s</i> )
30	1.07 ( <i>d</i> ; 6.8)	1.00 ( <i>d</i> ; 6.3)	
2-OH <sup>‡</sup>	5.21 ( <i>br s</i> )	5.21 ( <i>br s</i> )	5.49 ( <i>br s</i> )
3-OH <sup>‡</sup>	5.08 ( <i>br s</i> )	5.08 ( <i>br s</i> )	5.16 ( <i>br s</i> )
20-OH			3.40 ( <i>br s</i> )
22-OH	3.66 ( <i>br s</i> )		

\* Chemical shifts are reported as ppm ( $\delta$ ) from TMS in CDCl<sub>3</sub>, signal multiplicity and coupling constant (Hz) are in parentheses.

<sup>†</sup>, <sup>‡</sup> may be interchanged.

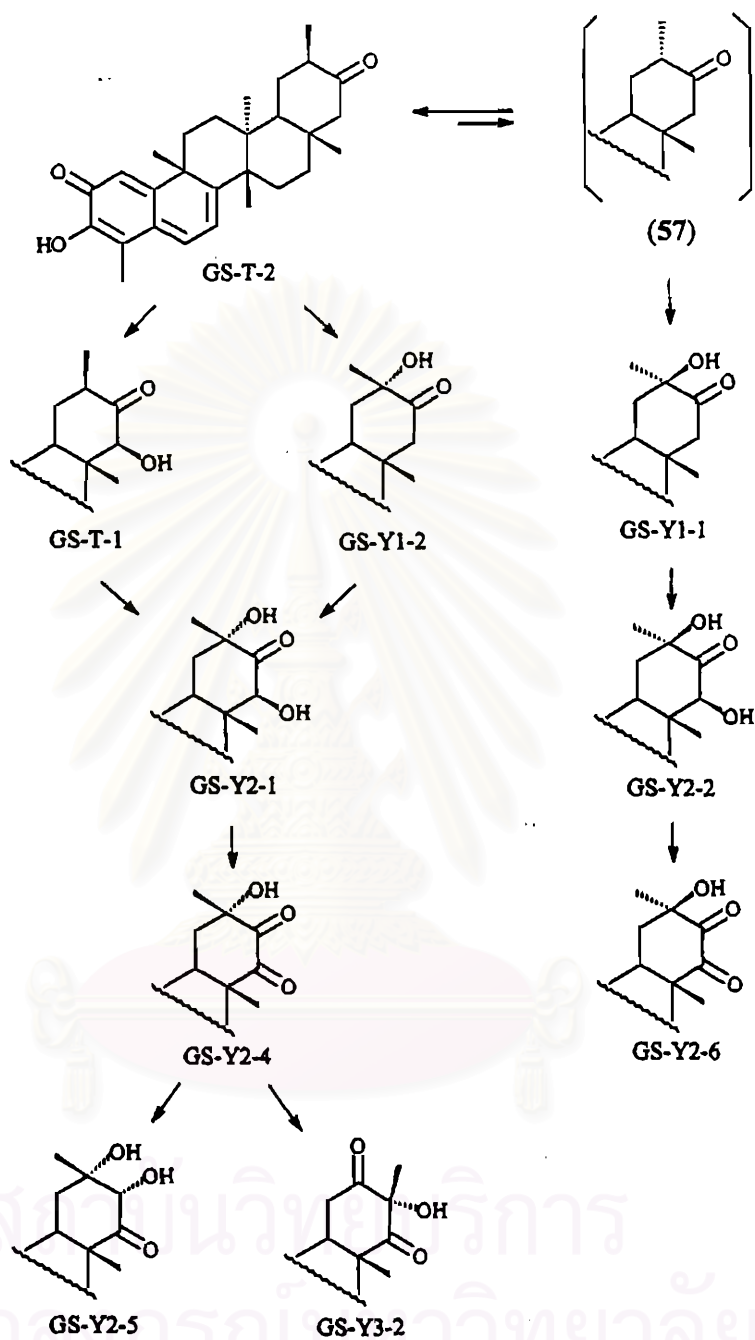
## 2. Proposed biogenesis of the isolated compounds

Structures of all isolated compounds varied only in ring E. Their biogenetic relationships could be explained by the sequential reactions outlined in Schemes 20 and 21.

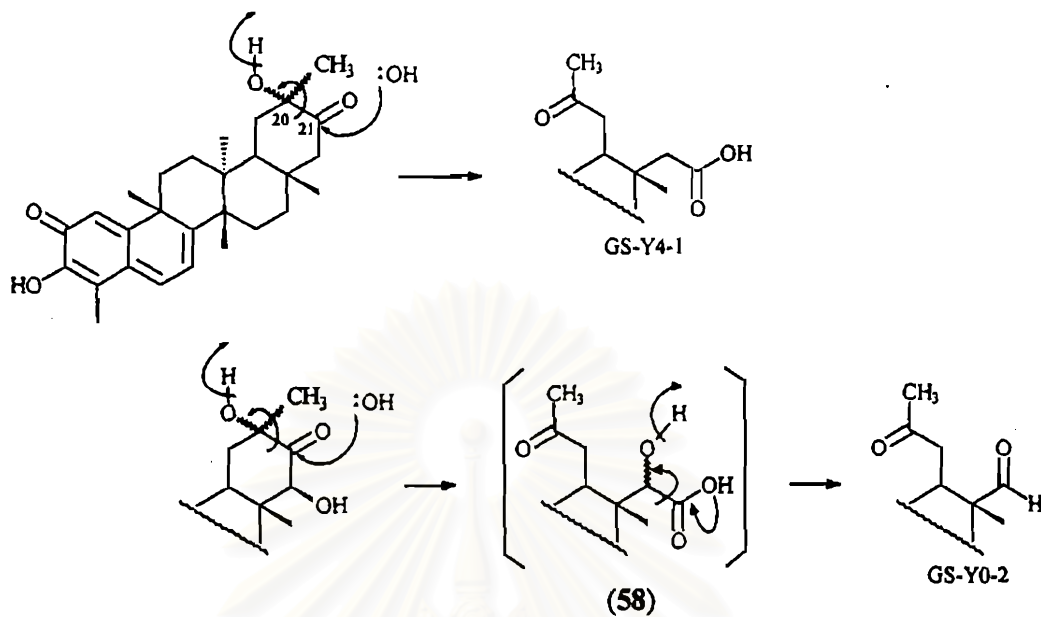
Oxidation was the main proposed biotransformation. The 1,2-methyl migration involved in biogenesis of GS-Y3-2. The epimerization between 20 $\alpha$  and 20 $\beta$ -CH<sub>3</sub> of GS-T-2 or tingenone (15) was similar to that suggested for balaenol type quinone-methide triterpenes<sup>49</sup>. However, its 20-epimer, isotingenone (57), has never been encountered in nature.

The most interesting biogenesis was that of the *E-seco* ring compounds. Hydroxylation at C-21, concomitant with the oxidation at C-20 of 20-hydroxy derivatives of tingenone, led to the C<sub>20</sub>-C<sub>21</sub> bond breaking. GS-Y4-1 (53) might be directly derived from GS-Y1-1 or its 20-epimer, whereas  $\alpha$ -hydroxy acid (58), the intermediate from the reaction of GS-Y2-1 or its 20-epimer would be subsequently decarboxylated to give GS-Y0-2 (52).





Scheme 21. Proposed biogenetic relationships of compounds in "T", "Y1", "Y2" and "Y3" series.

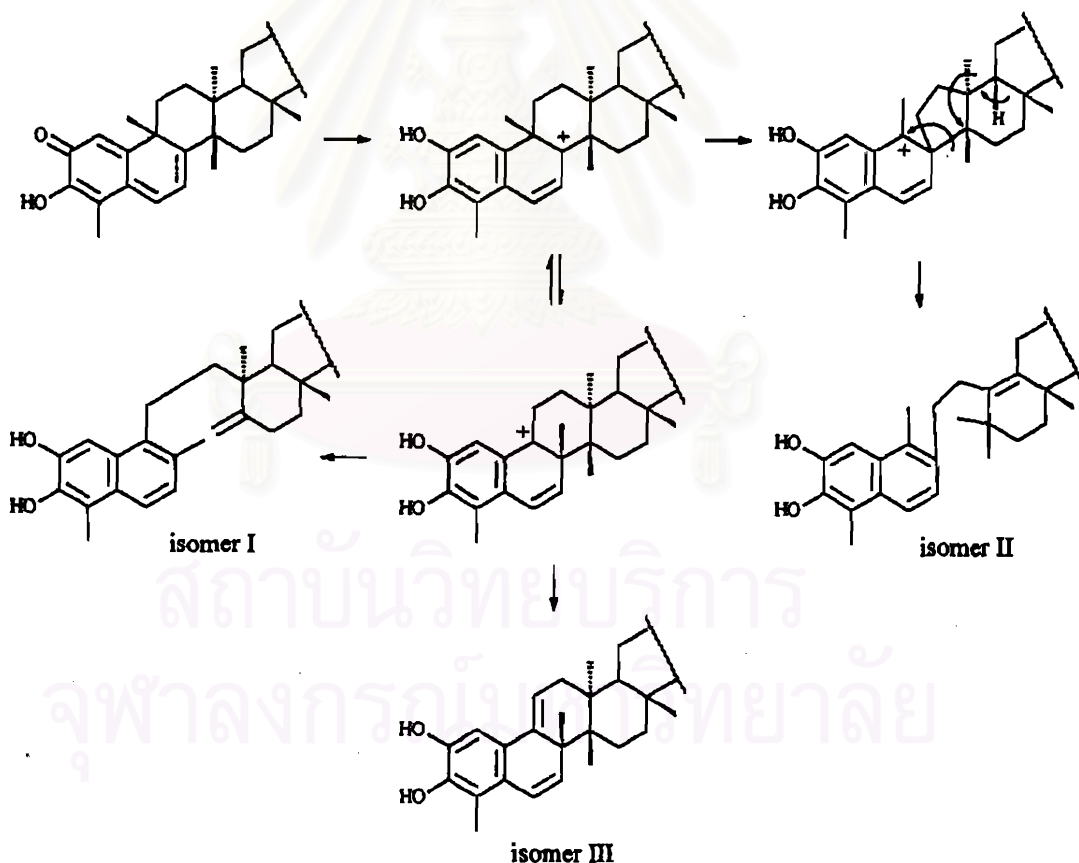


Scheme 22. Proposed biogenetic pathways of GS-Y0-2 and GS-Y4-1.

สถาบันวิทยบริการ  
จุฬาลงกรณ์มหาวิทยาลัย

### 3. Acid stability of GS-T-1, GS-T-2 and GS-Y1-1

Three main chemical constituents, GS-T-1 (1), GS-T-2 (15) and GS-Y1-1 (2), were tested for their stability in acidic condition. Although there were several experiments of acid-catalyzed rearrangement of quinone-methide triterpenes, but  $\text{H}_2\text{SO}_4$  refluxing was the only condition employed. Three rearrangement products were obtained as shown in Scheme 23. Isomers I and II were formed under strong acidic condition (2 N.  $\text{H}_2\text{SO}_4$ ), while isomer III was found only when diluted  $\text{H}_2\text{SO}_4$  was used<sup>48,131-132,156</sup>. This study intended to imitate the acidic condition of the stomach, however only the acid (HCl) and acidity (pH 2) were likely.



Scheme 23. Acid-rearranged products of quinone-methide triterpenes.

After the sample compounds were treated with acid, UV absorption at the selected wavelength of substrates (420 nm) and products (306 nm) were measured immediately and at intervals. The UV data were then analyzed for the concentrations through their molar absorptivity ( $\epsilon$ ) (Tables 13-15).

The amount of all sample compounds decreased rapidly in the first 20 minutes then slowed down, whereas their products exhibited similar feature in opposite direction. The reaction appeared to be complete within 60 minutes (Figure 28).

Additional information gathered from this study revealed GS-T-1 (1), GS-T-2 (15) and GS-Y1-1 (2) to be very unstable under acidic condition, even when no heating was included in the reaction condition. However, isomer III was still the main product, in accordance with the NMR interpretation discussed in section 1. Therefore, if quinone-methide triterpenes were orally administrated, isomer III should be the main from of the compounds in the stomach.

Table 13. Amount of GS-T-1 (1) and GS-T-1-ACID (54) in acid reaction at intervals.

Time (min)	GS-T-1 (1)			GS-T-1-ACID (54)		
	A 420 nm	Conc. (mg/ml)	% per starting GS-T-1	A 306 nm	Conc. (mg/ml)	% per starting GS-T-1
0	1.666	0.0594	100.00	0.000	0.0000	0.00
5	0.895	0.0319	53.72	0.421	0.0283	47.70
10	0.433	0.0154	25.99	0.563	0.0379	63.79
15	0.089	0.0032	5.34	0.668	0.0450	75.69
20	0.054	0.0019	3.20	0.695	0.0467	78.62
30	0.010	0.0004	0.60	0.717	0.0483	81.24
60	0.008	0.0003	0.48	0.755	0.0508	85.54

Table 14. Amount of GS-T-2 (15) and GS-T-2-ACID (55) in acid reaction at intervals.

Time (min)	GS-T-2 (15)			GS-T-2-ACID (55)		
	A 420 nm	Conc. (mg/ml)	% per starting GS-T-2	A 306 nm	Conc. (mg/ml)	% per starting GS-T-2
0	1.374	0.0309	100.00	0.000	0.0000	0.00
5	0.930	0.0209	67.69	0.377	0.0162	52.50
10	0.603	0.0136	43.89	0.482	0.0207	67.12
15	0.395	0.0089	28.75	0.545	0.0234	75.89
20	0.258	0.0058	18.78	0.585	0.0251	81.46
30	0.115	0.0026	8.37	0.639	0.0275	88.98
60	0.050	0.0011	3.64	0.652	0.0280	90.79

Table 15. Amount of GS-Y1-1 (2) and GS-Y1-1-ACID (56) in acid reaction at intervals.

Time (min)	GS-Y1-1 (2)			GS-Y1-1-ACID (56)		
	A 420 nm	Conc. (mg/ml)	% per starting GS-T-1	A 306 nm	Conc. (mg/ml)	% per starting GS-Y1-1
0	1.137	0.0337	100.00	0.000	0.0101	0.00
5	0.667	0.0364	58.66	0.151	0.0191	52.40
10	0.335	0.0214	29.46	0.284	0.0249	68.27
15	0.184	0.0107	16.18	0.370	0.0276	75.84
20	0.080	0.0059	7.04	0.411	0.0299	82.11
30	0.044	0.0026	3.87	0.464	0.0312	85.62
60	0.020	0.0014	1.76	0.480	0.0322	88.57

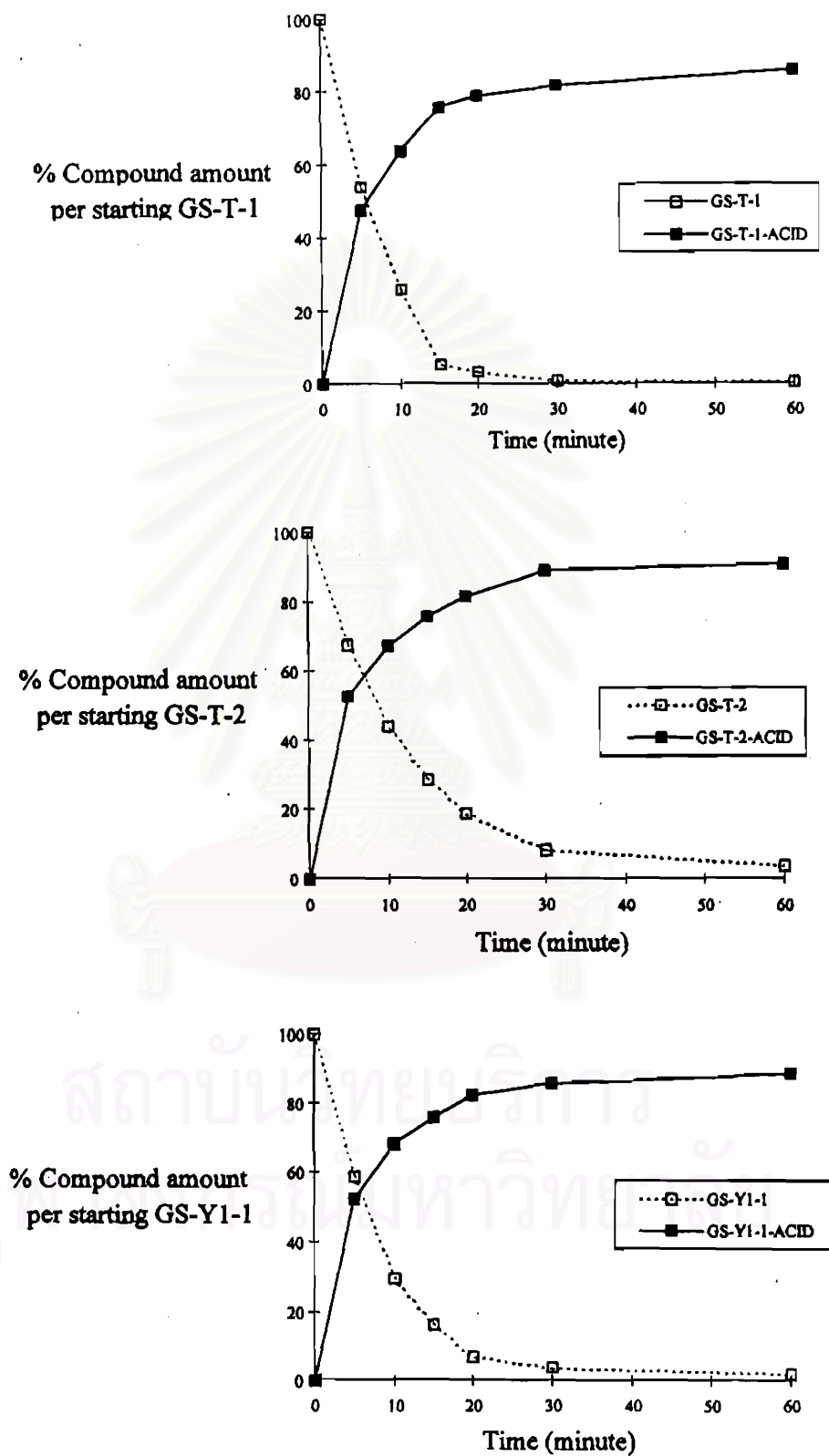


Figure 28. Amount of each substrate and its acid-rearranged product at intervals.

#### 4. Lipophilicity of isolated and acid-rearranged compounds

Lipophilic character is an important factor for the penetration of compounds into cells, hence, affecting its biological activity. To determine the lipophilicity, the TLC method, in which the impregnated liquid paraffin was illustrated as oil phase and developed with aqueous mobile phase, has a number of advantages over the conventional *n*-octanol/water partition. It is easier, quicker and required very small amount of sample compounds. Also, several compounds can be simultaneously tested<sup>151</sup>.

In this study, when the mobile phase was distilled water alone, all tested compounds did not move from the starting line. Thus, adding acetone to the mobile phase was necessary to obtain accurate *R<sub>f</sub>* values in the range of 0.2-0.8<sup>151</sup>. All compounds gave satisfactory *R<sub>f</sub>* values with 50-70% acetone, except that of GS-Y4-1 which was 30-50% (Table 16). *R<sub>f</sub>* values were then transformed to *R<sub>m</sub>* values (Table 17). These ranges of acetone composition exhibited good linear relationship with *R<sub>m</sub>* values. Extrapolated *R<sub>m</sub>* values could be obtained from equations calculated by means of *R<sub>m</sub>* values determined with acetone concentrations as shown in Table 18. The intercept was the extrapolated *R<sub>m</sub>* values calculated at 0% acetone mobile phase and represented lipophilicity of the compounds in the comparison. The slopes showed that the equations described a series of almost parallel straight lines and thus, validated this experiment.

สถาบันวิทยบริการ  
จุฬาลงกรณ์มหาวิทยาลัย

Table 16.  $R_f$  values of compounds from *Glyptopetalum sclerocarpum* Laws. on liquid paraffin impregnated TLC developed with mobile phases at various compositions of acetone in distilled water.

Acetone (%)	$R_f$											
	GS-T-1 (1)	GS-T-2 (15)	GS-Y1-1 (2)	GS-Y1-2 (45)	GS-Y2-1 (46)	GS-Y2-2 (47)	GS-Y2-4 (49)	GS-Y0-2 (52)	GS-Y4-1 (53)	GS-T-1-ACID (54)	GS-T-2-ACID (55)	GS-Y1-1-ACID (56)
10	0.00	0.00	0.00	0.00	0.00	0.00	0.00	0.00	0.02	0.00	0.00	0.00
20	0.00	0.00	0.00	0.00	0.00	0.00	0.00	0.00	0.09	0.00	0.00	0.00
30	0.00	0.00	0.00	0.00	0.00	0.00	0.00	0.00	0.49	0.00	0.00	0.00
40	0.05	0.08	0.11	0.09	0.13	0.22	0.14	0.12	0.77	0.05	0.03	0.07
50	0.15	0.20	0.25	0.23	0.30	0.38	0.30	0.27	0.83	0.18	0.13	0.22
60	0.35	0.42	0.50	0.45	0.45	0.54	0.48	0.44	1.00	0.39	0.34	0.44
70	0.54	0.60	0.67	0.61	0.61	0.69	0.61	0.63	1.00	0.55	0.50	0.61
80*												

\* All compounds were at the solvent front.

Table 17.  $R_m$  values calculated from  $R_f$  data in Table 16. ( $R_m = \log (1/R_f - 1)$ )

Acetone (%)	$R_m$											
	GS-T-1 (1)	GS-T-2 (15)	GS-Y1-1 (2)	GS-Y1-2 (45)	GS-Y2-1 (46)	GS-Y2-2 (47)	GS-Y2-4 (49)	GS-Y0-2 (52)	GS-Y4-1 (53)	GS-T-1-ACID (54)	GS-T-2-ACID (55)	GS-Y1-1-ACID (56)
30									0.02			
40									-0.52			
50	0.75	0.60	0.48	0.52	0.37	0.21	0.37	0.43	-0.69	0.66	0.82	0.55
60	0.27	0.14	0.00	0.09	0.09	-0.07	0.03	0.10		0.19	0.29	0.10
70	-0.07	-0.18	-0.23	-0.21	-0.19	-0.35	-0.19	-0.23		-0.09	0.00	-0.19



Table 18. TLC equations for extrapolated  $R_m$  values.(a = intercept, b = slope,  $r^2$  = correlation coefficient)

Compound	TLC equation		
	a (= $R_m$ )	b	$r^2$
GS-T-1 (1)	2.5232	-0.0389	0.99
GS-T-2 (15)	2.7864	-0.0411	0.99
GS-Y1-1 (2)	2.4106	-0.0392	0.98
GS-Y1-2 (45)	2.3452	-0.0369	0.99
GS-Y2-1 (46)	1.7737	-0.0281	1.00
GS-Y2-2 (47)	1.6121	-0.0280	1.00
GS-Y2-4 (49)	1.7562	-0.0281	0.99
GS-Y4-1 (53)	1.0133	-0.0353	0.91
GS-Y0-2 (52)	2.0911	-0.0332	1.00
GS-T-1-ACID (54)	2.4923	-0.0373	0.98
GS-T-2-ACID (55)	2.8479	-0.0413	0.97
GS-Y1-1-ACID (56)	2.3852	-0.0372	0.99

GS-T-2 (15) was the most lipophilic among isolated compounds. Lipophilicity decreased through the order of oxygenated substitutions. The *E-seco* compounds exhibited unpredictable lipophilicity. That of GS-Y0-2 (52) was between that of one and two oxygenated tingenone derivatives, while GS-Y4-1 (53) possessing carboxylic acid terminal was the most hydrophilic compound. The different lipophilicity between 20-epimers (compounds (2)-(45) and (46)-(47)) suggested that stereochemistry was an important factor of compound lipophilicity. The acid-rearrangement reaction did not significantly change the lipophilicity of these compounds (compounds (1)-(54), (15)-(55) and (2)-(56)).

สถาบันวิทยบริการ  
จุฬาลงกรณ์มหาวิทยาลัย

## 5. Biological activity

Brine-shrimp lethality (BSL) test was the assay chosen for determining the bioactivity of isolated fractions and pure compounds, because its result corresponded to those assays of tumor cell-line cytotoxic, insecticide, antimicrobial activities, etc,<sup>153,157</sup> which covered major spectrum of activities of the compounds from plants of the Celastraceae. Antimicrobial assay was specifically performed in order to support the indigenous use of the plant to treat infectious disease. Their results were presented in Tables 20 and 21.

All compounds gave positive results to BSL test and exhibited antimicrobial activity against gram-positive bacteria, fungi and only a gram-negative bacterium, *K. pneumoniae*. Yeasts and most gram-negative bacteria were unsusceptible to these compounds. The isolated compounds (compounds (1), (2) and (15)) displayed quite stronger BSL than their acid-rearranged products (compound (54), (55) and (56)), while antimicrobial activity seemed to be lost by the acid reaction. GS-T-2 or tingenone (15) was the most active compound in both tests. Its antibacterial and antifungal potency were comparable to the commercial drugs, tetracycline and tolnaftate, respectively.

GS-T-2 (15) was known for its potent activity against gram-positive bacteria<sup>34</sup>, whereas *in vitro* cytotoxicity of GS-T-1 (1), GS-T-2 (15) and GS-Y1-1 (2) have been reported<sup>13,15-16,28,33</sup>. Their potency against KB cell-line corresponded to the result from BSL test in this study (Table 19). GS-T-2 (15) exhibited 10 and 3 times more activity than GS-T-1 (1) and GS-Y1-1 (2), respectively. Therefore, determining on BSLD<sub>50</sub> was a satisfactory and easy bench-top bioassay for these compound derivatives.

Table 19. The brine-shrimp lethality and KB cell-line cytotoxicity of GS-T-1 (1), GS-T-2 (15) and GS-Y1-1 (2)

Compound	BSLD <sub>50</sub>	KB cell-line cytotoxicity	
		ED <sub>50</sub> (µg/ml) *	ED <sub>50</sub> (µg/ml) †
GS-T-1 (1)	4.73	2.50	
GS-T-2 (15)	0.48	0.27	0.5
GS-Y1-1 (2)	1.25		1.7

\* Data from reference [28].

† Data from reference [16].

Mechanisms of the toxic action of quinone-methide triterpenes have been postulated. In subcellular bioassay, quinone-methide triterpenes could interact with DNA<sup>119</sup>. They also acted as a classical uncoupler of mitochondrial oxidative phosphorylation by reacting at sulfhydryl groups on inner membrane<sup>17</sup>. These actions might block macromolecule biosyntheses in mammalian and parasitic cells<sup>69,133,137-138</sup>. Inhibitory effect on mitochondrial electron transport system also corresponded to that studied on whole microorganism cells<sup>35</sup>. Even though bacteria have no mitochondria, the oxidative phosphorylation reaction in cell membrane might be the site of action.



สถาบันวิทยบริการ  
จุฬาลงกรณ์มหาวิทยาลัย

Table 20. Diameter (mm) of clear zones in the assay of compounds from *Glyptopetalum sclerocarpum* Laws. against different microorganisms.

Microorganism	Concentration of compound in the hole* ( $\mu\text{g/ml}$ )													
	GS-T-1		GS-T-2		GS-Y1-1		GS-Y1-2		GS-Y2-1		GS-Y2-2		GS-Y2-4	
	(1)	(1)	(15)	(15)	(2)	(2)	(45)	(45)	(46)	(46)	(47)	(47)	(48)	(48)
	50	100	50	100	50	100	50	100	50	100	50	100	50	100
<i>B. cereus</i>	15.2	16.2	14.3	14.7	16.5	17.9	15.1	15.8						
<i>B. subtilis</i>	16.5	17.2	16.1	16.4	18.7	19.6	16.9	17.8	16.3	19.1	12.9	17.9	16.7	20.2
<i>S. lutea</i>	18.9	20.2	16.9	17.8	18.5	20.0	16.4	17.9						
<i>S. aureus</i>	15.4	16.9	13.5	14.2	17.2	18.2	14.6	15.4	15.9	16.9	13.3	14.9	15.9	17.7
<i>E. coli</i>	NI†	NI	NI	NI	NI	NI	NI	NI	NI	NI	NI	NI	NI	NI
<i>K. pneumoniae</i>	14.4	15.3	11.8	12.8	12.3	14.7	11.0	11.8	13.4	13.8	11.4	13.0	13.4	13.9
<i>Ps. Aeruginosa</i>	NI	NI	NI	NI	NI	NI	NI	NI	NI	NI	NI	NI	NI	NI
<i>Sal. typhimurium</i>	NI	NI	NI	NI	NI	NI	NI	NI	NI	NI	NI	NI	NI	NI
<i>C. albicans</i>	NI	NI	NI	NI	NI	NI	NI	NI	NI	NI	NI	NI	NI	NI
<i>Sc. Cerevisiae</i>	NI	NI	NI	NI	NI	NI	NI	NI	NI	NI	NI	NI	NI	NI
<i>M. gypseum</i>	11.2	14.0	9.8	11.4	16.5	18.5	10.4	13.2	NI	10.5	NI	NI	10.5	14.4
<i>T. rubrum</i>	9.8	11.7	8.2	8.5	8.8	11.0	8.2	9.2						

\* Diameter of the hole was 6 mm.

† NI = no inhibition zone was observed.

Table 20. (Continued)

Microorganism	Concentration of compound in the hole* ( $\mu\text{g/ml}$ )											
	GS-Y0-2 (52)		GS-Y4-1 (53)		GS-T-1- ACID (54)		GS-T-2- ACID (55)		GS-Y1-1- ACID (56)		Tetracycline HCl	Tolnaftate
	50	100	50	100	50	100	50	100	50	100	600	600
<i>B. cereus</i>					9.5	10.3	9.4	9.7	8.6	10.1	29.7	
<i>B. subtilis</i>	14.8	19.6	15.7	21.3	10.4	11.8	10.1	11.4	10.1	11.7	37.5	
<i>S. lutea</i>					8.8	10.8	8.5	9.2	9.5	10.5	33.5	
<i>S. aureus</i>	13.7	16.0	16.8	21.7	8.5	9.9	8.4	9.0	7.6	9.0	30.5	
<i>E. coli</i>	NI	NI	NI	NI	NI	NI	NI	NI	NI	NI	22.6	
<i>K. pneumoniae</i>	11.4	13.9	14.3	16.1	8.0	10.0	8.8	9.3	7.5	9.2	19.4	
<i>Ps. aeruginosa</i>					NI	NI	NI	NI	NI	NI	NI	
<i>Sal. typhimurium</i>					NI	NI	NI	NI	NI	NI	23.4	
<i>C. albicans</i>	NI	NI	NI	NI	NI	NI	NI	NI	NI	NI		
<i>Sc. cerevisiae</i>					NI	NI	NI	NI	NI	NI		
<i>M. gypseum</i>	8.1	10.0	NI	NI	NI	NI	NI	NI	NI	NI		38.0
<i>T. rubrum</i>					NI	NI	NI	NI	NI	NI		36.5

\* Diameter of the hole was 6 mm.

; NI = no inhibition zone was observed.

Table 21. MIC and BSLD<sub>50</sub> values of compounds from *Glyptopetalum sclerocarpum* Laws.

Organism	MIC value and BSLD <sub>50</sub> (µg/ml)						
	GS-T-1 (1)	GS-T-2 (15)	GS-Y1-1 (2)	GS-Y1-2 (45)	GS-Y2-1 (46)	GS-Y2-2 (47)	GS-Y2-4 (49)
<i>B. cereus</i>	1	1	2	2	>8	>8	8
<i>B. subtilis</i>	1	0.5	2	2	8	8	4
<i>S. lutea</i>	1	1	4	2	>8	>8	8
<i>S. aureus</i>	2	2	4	4	>8	>8	8
<i>K. pneumoniae</i>	4	4	8	8	>8	>8	>8
<i>M. gypseum</i>	4	8	4	4	>8	>8	>8
Brine shrimp	4.73	0.48	1.25	0.85	7.14	21.16	10.70

Table 21. (Continued)

Organism	MIC value and BSLD <sub>50</sub> (µg/ml)						
	GS-Y0-2 (52)	GS-Y4-1 (53)	GS-T-1- ACID (54)	GS-T-2- ACID (55)	GS-Y1-1- ACID (56)	Tetracycline HCl	Tolnaftate
<i>B. cereus</i>	8	8	64	>64	64	1	
<i>B. subtilis</i>	8	8	64	>64	32	0.5	
<i>S. lutea</i>	>8	>8	>64	>64	>64	4	
<i>S. aureus</i>	>8	8	>64	>64	>64	2	
<i>K. pneumoniae</i>	>8	>8	>64	>64	>64	4	
<i>M. gypseum</i>	8	>8	>64	>64	>64		8
Brine shrimp	3.71	41.86	26.91	69.85	3.16	>100	>100

## 6. Structure-activity relationships (SAR)

Correlation of the structure and their bioassays results indicated some clear SAR, possibly due to a biomolecule interaction-based mode of action of the compounds. On this basis, a more detailed analysis of possible SAR was undertaken using computer-based molecular modeling methodology. The most active compound, GS-T-2 or tingenone (15), was used as the basic structure.

### 6.1) SAR of tingenone derivatives

#### 6.1.1) Toxicity to brine shrimp

Hydroxylation either at C-20 or C-22 of tingenone (15) diminished BSL activity (Table 22). The 22 $\beta$ -hydroxyl derivative (1) displayed similar activity to the compound with ring E opening to a keto- and an aldehyde side chain (compound (52)). However, if the side chains were a ketone and a carboxylic acid (compound (53)), activity was about 100 times less than the parent compound. This observations indicated that ring E was not necessary for the activity. Instead, it was the functional groups in this region that played an important role.

All compounds possess at least one carbonyl group in ring E region. Their minimized structures (Figures 7, 10, 11, 14, 17, 18, 21, 24, 26, 29, 30 and 31) were identical in that this functional group was spatially laid below or out of the molecule in ring E region, and thus, generated electrostatic potential in this area which might be essential to molecule-biomolecule interaction. Importance of oxygenated functionalities at ring E of quinone-methide triterpenes on bioactivities have also been suggested by some research groups<sup>33,34</sup>.

Based on this hypothesis, other oxygenated functional groups in the region of ring E should enhanced the activity. But in reality, neither of them did. Increment in the number of oxygenated substitutions generally resulted in less lipophilicity of the molecule which might influence bioactivity. A plot between  $\log(1/BSLD_{50})$  and lipophilicity ( $Rm$ ) of all compounds (Figure 32) showed the tendency of this directly correlated factor

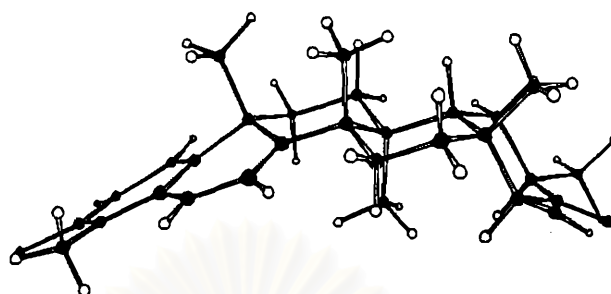


Figure 29. Most stable conformation of GS-T-1 (1), calculated by MM2 force field (48.672 kcal/mole).

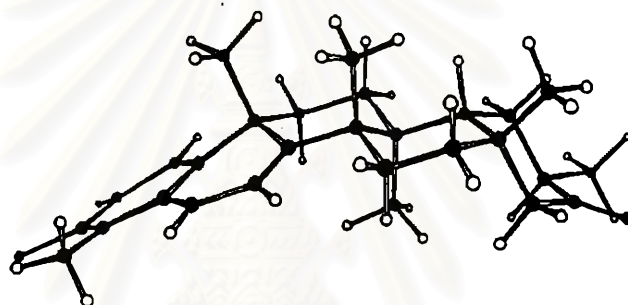


Figure 30. Most stable conformation of GS-T-2 (15), calculated by MM2 force field (49.332 kcal/mole).

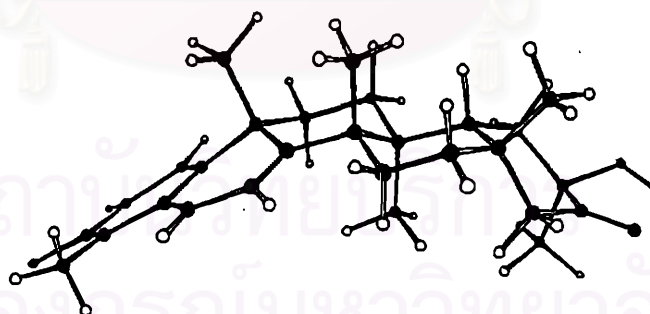
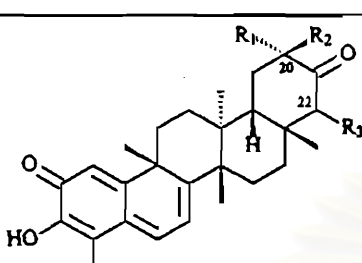
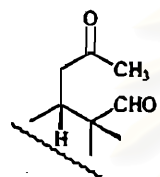
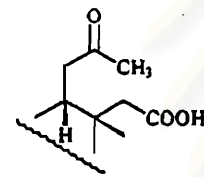


Figure 31. Most stable conformation of GS-Y1-1 (2), calculated by MM2 force field (53.445 kcal/mole).



Table 22. Correlations between structures of ring E of tingenone derivatives and their brine-shrimp lethality.

Structure	Structure			BSLD <sub>50</sub> ( $\mu\text{g/ml}$ )	
	R <sub>1</sub> (20 $\alpha$ )	R <sub>2</sub> (20 $\beta$ )	R <sub>3</sub> (22)		
	GS-T-2 (15)	H	CH <sub>3</sub>	H	0.48
	GS-T-1 (1)	H	CH <sub>3</sub>	$\beta$ -OH	4.73
	GS-Y1-2 (45)	OH	CH <sub>3</sub>	H	0.85
	GS-Y1-1 (2)	CH <sub>3</sub>	OH	H	1.25
	GS-Y2-1 (46)	OH	CH <sub>3</sub>	$\beta$ -OH	7.14
	GS-Y2-2 (47)	CH <sub>3</sub>	OH	$\beta$ -OH	21.16
	GS-Y2-4 (49)	OH	CH <sub>3</sub>	=O	10.70
	GS-Y0-2 (52)				3.71
	GS-Y4-1 (53)				41.86

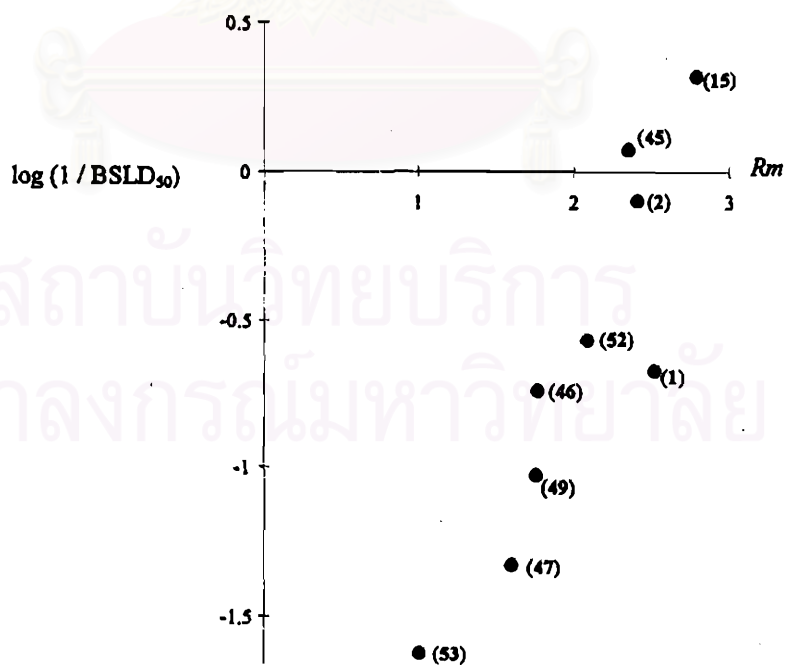


Figure 32. Correlation between toxicity to brine shrimp (log 1/BSLD<sub>50</sub>) and lipophilicity (*R*<sub>m</sub>) of tingenone derivatives.

Different influences on activity were found between hydroxylation at C-20 and C-22. Lipophilicity among mono-hydroxylated derivatives of tingenone was not much different, though certainly less than that of tingenone (15). However, toxicity of the 20-hydroxyl derivatives, (2) and (45), was only partially lost, while 22 $\beta$ -hydroxyl derivative (1) was 10 times less active than its parent compound (Table 22). According to the minimized structures of both 20 $\alpha$ - and 20 $\beta$ -hydroxyl derivatives (Figures 7 and 31), their hydroxyl groups were spatially laid behind ring E (region B in Figure 33). Electrostatic potential in this area might be important. However, similar factor in the area of C-22 in front of ring E (region C) should be undesirable.

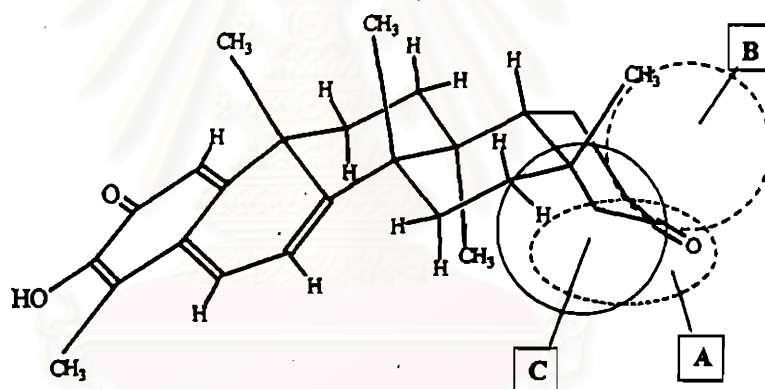


Figure 33. Proposed molecular properties required for bioactivities of ring E of tingenone derivatives.

- Toxicity to brine shrimp  
(A), (B) = electronic regions (C) = hydrophobic region
- Antimicrobial activity against gram-positive bacteria and fungi  
(A), (C) = electronic regions (B) = hydrophobic region

Comparison between the two same lipophilicity but different oxygenated functional group at C-22, compound (46) with a hydroxyl group and compound (49) with carbonyl group, revealed the carbonyl one to be less accommodated for the activity (Table 22).

The two different binding regions mentioned above did not much affected the activity of the two *E-seco* compounds, (52) and (53). Conceivably, their side chains rotated and allowed the oxygenated functional groups to be in satisfactory positions. Lipophilicity should be the main factor that influenced the activity of these compounds.

Although electrostatic potential in the region of ring E of quinone-methide triterpenes was important for molecule-biomolecule binding, but benefit of this factor through oxidative substitutions would be compensated by the lower lipophilicity of the oxygenated molecules. Since there are at least two barriers in the cellular level, that of cell membrane and nuclear or mitochondrial membrane, only the compounds with optimal lipophilicity can to successfully penetrate from the environment around the organism to the target sites in the cells.

#### 6.1.2) Antimicrobial activity

Antimicrobial activity of these compounds, unlike toxicity to brine-shrimps, could only be slightly correlated to their lipophilicity (Figure 34), although the type and position of oxygenated functional groups on ring E were rather significant. However, electrostatic potential in the region A as shown in Figure 33 might still be necessary.

##### 6.1.2.1) Antibacterial activity

*Vice versa* toxicity to brine shrimp, substitution of a hydroxyl group on C-20 of tingenone resulted in less antibacterial activity (compounds (2) and (45)) (Table 23), while hydroxylation at C-22 $\beta$  (compound (1)) produced comparable effect. According to the minimized structures, 20 $\alpha$ -or 20 $\beta$ - hydroxyl groups would be positioned in region B (Figure 33), indicating that electrostatic potential at this area might interfere with molecule-biomolecule binding. This observation agreed with the activity of (52), of which a ketone side chain was laid in this region. Compounds (52) and (1) had no observable difference in lipophilicity, but the activity of the former was 8 times weaker than the latter.

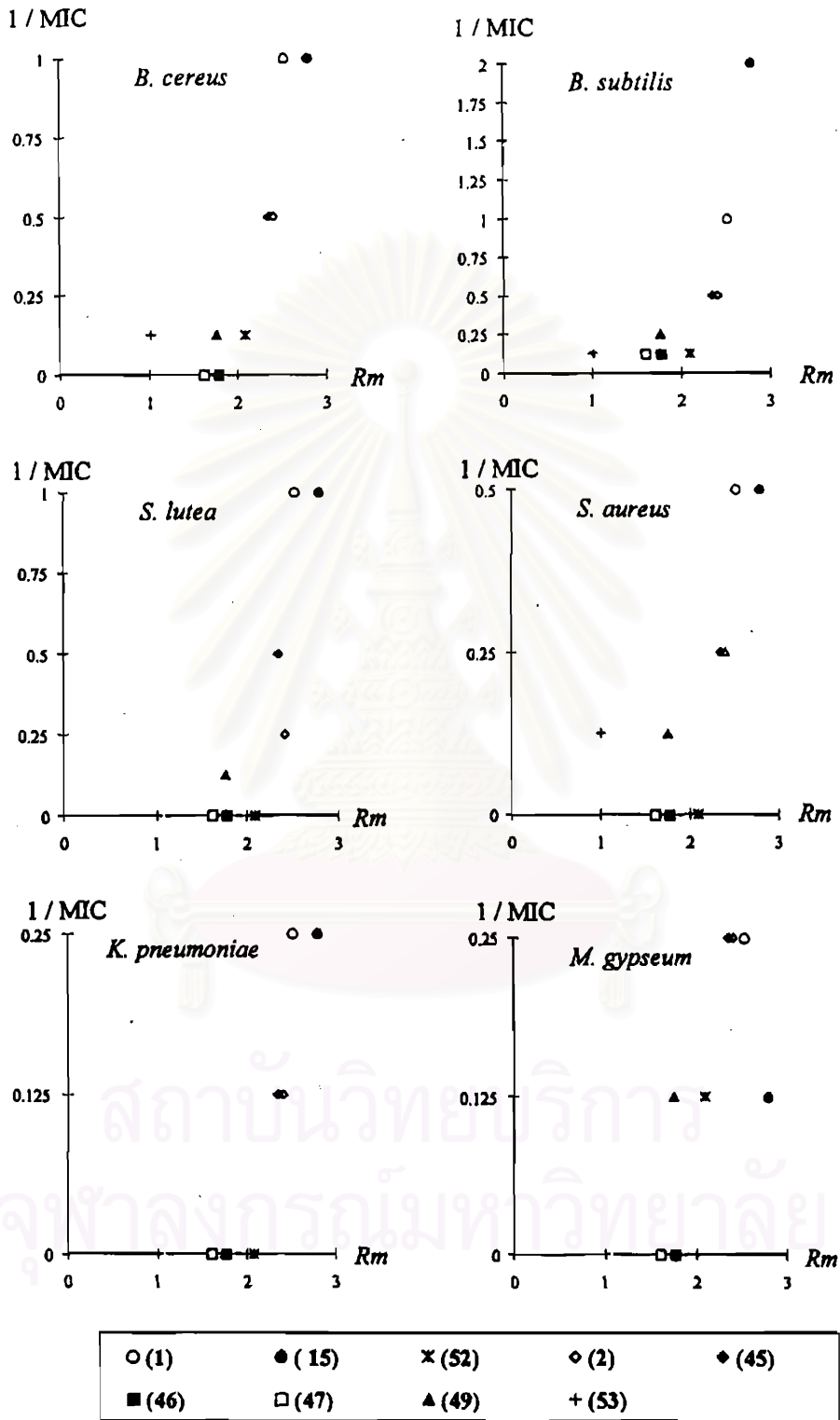
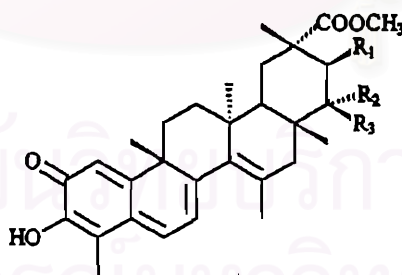


Figure 34. Correlation between antimicrobial activity against different microorganisms (1/MIC) and lipophilicity (*Rm*) of tingenone derivatives.



Not only with the 20-OH substitution, the less active compounds, (46), (47) and (49), could also be explained by their lipophilicity. Compound (49) exhibited slightly stronger activity than the others. It seemed that 22-carbonyl was more agreeable than 22-OH for the electronic-binding force. The importance of electrostatic potential in the area in front of ring E (region C, Figure 33) was supported by the activity of (53). Although its hydrophilicity and ketone side chain retarded the activity, the very strong electrostatic potential of carboxylic acid side chain at the appropriate position could summarily overcome them.

Based on these observations, electrostatic potential in the area of C-21 and C-22 of ring E would be concerned for the antibacterial activity of quinone-methide triterpenes. In agreement with the previously reported data of netzahualcoyone type of quinone-methide triterpenes<sup>34</sup>, potency of antibacterial activity against *S. aureus* increased in the order of netzahualcoyene (59), netzahualcoyonol (60), netzahualcoyondiol (61) and netzahualcoyone (43). Lipophilicity of the compounds played less important role because microorganisms contacted directly with them. Only cell wall and cytoplasmic membrane are the barriers that prevent compound from penetrating to its target sites in cytoplasmic membrane or at DNA.



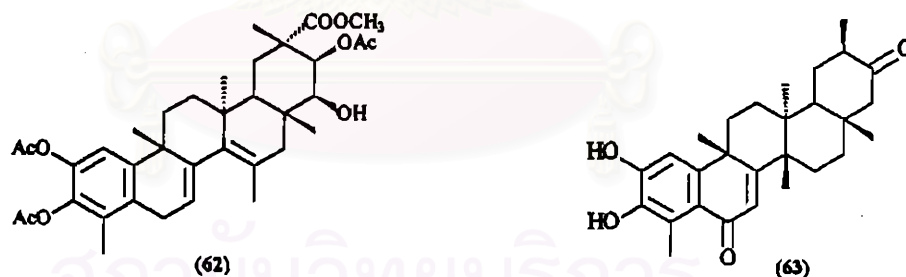
	R <sub>1</sub>	R <sub>2</sub>	R <sub>3</sub>
(59)	H	H	H
(60)	OH	H	H
(61)	OH	H	OH
(43)	OH	=O	

### 6.1.2.2) Antifungal activity

SAR for antifungal activity resembled that of antibacterial, although compound lipophilicity played more important role owing to the existence of mitochondrial and nuclear membrane barriers. Moreover, cellulose composition in fungal cell wall might be the cause of less lipophilicity for optimal activity (Figure 34).

### 6.2) SAR of acid-rearranged compounds

The result from BSL assay in this study of acid-rearranged compounds appeared to agree with previously report against KB tumor cell-line<sup>51</sup>. Quinone-methide triterpenes with divinyl-phenolic system were less active than those with typical quinone-methide chromophore. Moreover, they lose nearly all of their antimicrobial activity (Table 21, page 120). However, antibacterial activity of two compounds with related phenolic systems, triacetyl-dihydro-netzahualcoyodiol (62) and 6-oxo-tingenone (63), were reported<sup>34,37</sup>, suggesting that significant decrease of the bioactivity of acid-rearranged compounds should be influenced by other factors than the phenolic system of ring A.



According to spatial arrangement of three acid-rearranged compounds, the divinyl-phenolic system significantly distorted the structure out of its original plane (Figure 35), possibly making them difficult to be fitted to the binding sites. Phenolic systems of active compounds (62) and (63) did not much affect the molecular plane (Figures 36 and 37), and thus, would not interfere with the molecule-biomolecule interaction. Acetyl groups of (62) did not involve in this proposed binding, since they were easily cut off by enzyme esterases, found normally in organisms.

These observations suggested that quinone-methide triterpenes with either quinone-methide or phenolic system could exhibit brine-shrimp lethality or cytotoxic and antimicrobial activities as long as they could spatially arrange their structure into proper areas.

Another hypothesis could also be proposed. According to the correlation between lipophilicity and activities of acid-rearranged compounds (Figures 38 and 39) which displayed inverse relation to those of their substrates (Figures 32 and 33), their binding sites were possibly different from typical quinone-methide triterpenes at the subcellular level. However, more studies should be performed to augment this limited data.

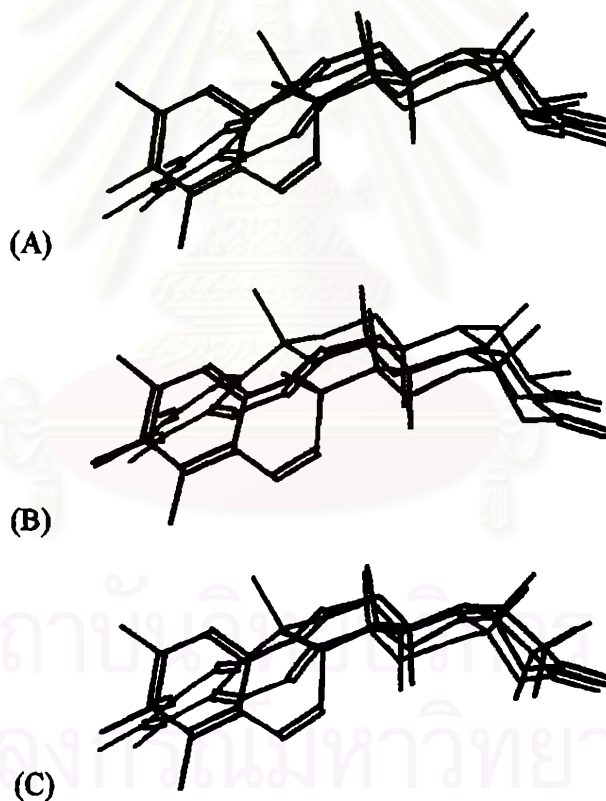


Figure 35. Superimposition of the preferred conformations of quinone-methide triterpenes (purple color) and its acid-rearranged products (green color).

(A) GS-T-1 (1) and GS-T-1-ACID (54)

(B) GS-T-2 (15) and GS-T-2-ACID (55)

(C) GS-Y1-1 (2) and GS-Y1-1-ACID (56)



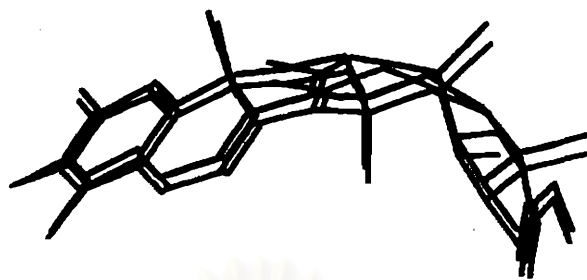


**Figure 36.** Superimposition of the preferred conformations of netzahualcodydiol (43) (purple color) and de-esterified structure of triacetyl-dihydro-netzahualcodydiol (62) (green color).

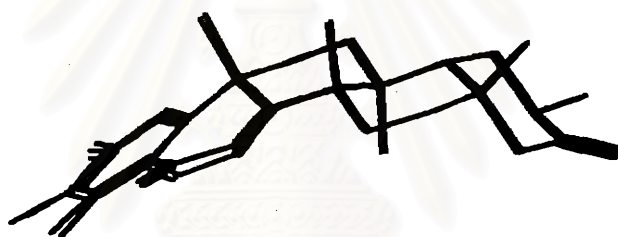


**Figure 37.** Superimposition of the preferred conformations of tingenone (15) (purple color) and 6-oxo-tingenone (63) (green color).

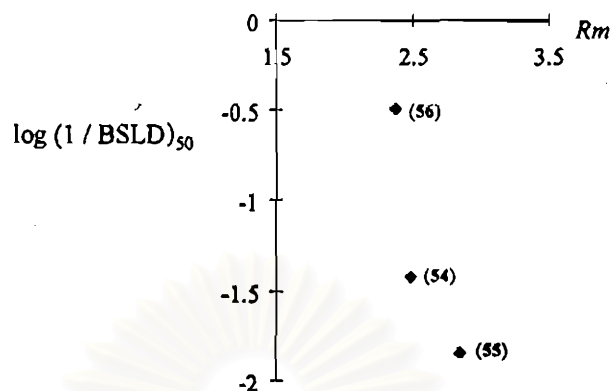


Figure 38. Correlation between toxicity to brine shrimp ( $\log 1/\text{BSLD}_{50}$ ) and lipophilicity ( $R_m$ ) of acid-rearranged compounds.

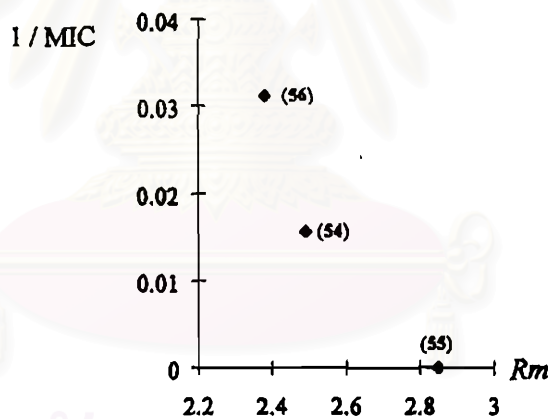


Figure 39. Correlation between antimicrobial activity against *B. subtilis* ( $1/\text{MIC}$ ) and lipophilicity ( $R_m$ ) of acid-rearranged compounds.